

Peter Sommereth Jaer
 NTNU

Norwegian University of
Science and Technology

Improvement of Thermodynamic Properties in Combustion Research Facility with Symmetrical Ignition Sources

Marine Technology

Submission date: October 2016

Supervisor: Eilif Pedersen, IMT

Co-supervisor: Vladimir Krivopolianskii, IMT

Norwegian University of Science and Technology
Department of Marine Technology

MASTER THESIS IN MARINE MACHINERY

FALL 2016

FOR

STUD.TECH. PETER SOMMERSETH JAER

TITLE OF THESIS: Improvement of Thermodynamic Properties in Combustion Research Facility with Symmetrical Ignition Sources

Work description:

The forecast for future energy demand is greatly dependent on both the increased world population and the welfare of the people. Reports released by various institutions predict an increase of 30-40 % in energy demand compared to the levels of today. This supply of energy is currently dominated by fossil fuel. According to International Maritime Organization (IMO) Greenhouse Gas (GHG) report from 2014 the shipping industry and its use of fossil fuel stands for 13% and 15 % of Sulfur Oxide (Sox) and Nitrogen Oxide (NOx) respectively and 3,1 % of the global carbon dioxide (CO₂) emission. Newly introduced emission regulation are the main driver for new technologies, which aim to reduce both fuel consumption and pollution in the marine sector. This reduction is directly linked to development in internal combustion engines and the study of injection and combustion is crucial in this aspect.

Various methods exist for simulating the conditions inside of a cylinder in a CI engine. The application of a constant volume combustion rig is suitable for research of injection and combustion. The constant volume combustion rig at MARINTEK has optical access allowing us to analyze both the injection and combustion. Together with pressure and temperature sensors, the test bed is convenient for evaluation of the thermodynamics and investigation of the combustion characteristics under controlled boundary conditions.

Previous tests with unsymmetrical combustion of the injected fuel led to a hypothesis that the test bed had an inhomogeneous temperature field inside the combustion rig after pre-combustion. This pre-combustion is used to get the thermodynamic conditions inside of the rig. A more symmetrical ignition of the gas mixture used for pre-combustion may eliminate these issues and provide a more accurate research tool in terms of improved boundary conditions and reproducibility of the test bed.

Several ignition systems were investigated during the pre-study before this present work. These include the conventional state of the art inductive ignition system from Motortech which has the capability of igniting several spark plugs simultaneously, as well as the more interesting, experimental, and alternative ignition system with corona discharge that was made in cooperation with the workshop Omega at NTNU. The remaining task is to implement the ignition systems and to design the electrode for the Corona discharge ignition systems and the other needed equipment for the combustion rig.

Scope of work:

1. Assist the work of assembling the combustion rig
2. Literature review on:
 - Ignition systems
 - Corona discharge
3. Design and manufacture an electrode for the corona driver
4. Implement both the conventional ignition system from Motortech and the Corona ignition system to the combustion rig
5. Compare the different ignition systems
 - Perform tests and compare the results with recorded data from the old ignition system
 - Lean out the gas mixture and find the lean limit for the different systems if time is available

The report shall be written in English and edited as a research report including a literature on ignition systems, introduction to corona discharge, design process, test procedures, conclusion including a proposal for further work.

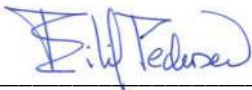
The Department of Marine Technology, NTNU, can use the results freely in its research work by referring to the students work.

The thesis should be submitted by 10.10.2016

Advisor: Associate Professor Eilif Pedersen

Co-advisor: PhD Candidate Vladimir Krivopolianskii

Department of Marine Technology 20.05.2016



*Eilif Pedersen
Associate Professor*

Abstract

The Constant Volume Combustion Chamber (CVCC) at the Combustion Laboratory at the Institute of Marine Technology has shown:

(I) Temperature related issues that reduce reproducibility within test series.

(II) The environment the vessel can simulate is not satisfactory in terms of density.

Previous results and observation with the use of a high-speed camera indicates that the CVCC has an inhomogeneous temperature field. This is due to unsymmetrical heat loss to the wall after pre-combustion, which is used to chemically heat the CVCC to reach the engine-like conditions. The CVCC can run up to a maximum of 100 [bar], which directly affects how much of the gas used for pre-combustion can be injected. The amount of the gas mixture that the old ignition system was capable of igniting cannot be increased substantially without reaching the pressure limit.

These issues were investigated in this present work by installing two types of ignition systems that both aimed to initiate a more symmetrical pre-combustion and to ignite leaner gas mixtures for the pre-combustion. The conventional inductive ignition system from Motortech has a dual spark configuration and an alternative ignition system using Corona Discharge made by Øystein Smith and fellow students at the Omega Workshop at the Norwegian University of Technology and Science (NTNU).

The experiment we conducted on the conventional ignition system indicated a higher maximum pressure level and a faster pre-combustion with a dual spark plug configuration compared to a single spark plug configuration, which could reduce the temperature gradient, but further experimentation is necessary to conclude on this issue. The system indicated an improved capability to ignite lean mixtures, during experiments where the volume fraction of Carbon Monoxide (CO) was reduced when the GMB was further pressurized with Nitrogen gas (N₂).

The corona discharge ignition system has promising properties as a symmetrical ignition source to address both issues presented. The challenge is to introduce the voltage into the CVCC without reaching the dielectric strength of the insulating material surrounding the conducting electrode. This would generate an arc between the electrode and the grounded CVCC. The initial experiments we conducted resulted in spark discharge and not corona discharge with all developed electrodes. Further development on the electrodes and a more controllable signal to drive the corona driver is necessary to get this ignition system working properly.

Sammendrag

Forbrenningskammeret med konstant volum på Forbrennings Laboratoriet ved Instituttet for Marin teknikk har vist følgende:

(I) temperaturrelaterte problemer som reduserer dens reproduserbarhet mellom eksperimenter, som er hovedmålet for denne type forskningsutstyr.

(II) Forholdene som forbrenningskammeret kan simulere er ikke tilfredsstillende i henhold til tetthet.

Tidligere resultater og observasjon med bruk av høyhastighetskamera har vist at forbrenningsriggen har et inhomogent temperaturfelt. Dette skyldes usymmetriske varmetap til veggen i forbrenningskammeret etter pre-forbrenning, som benyttes for kjemisk oppvarme forbrenningskammeret til motorlignende tilstander. Dette forbrenningskammeret tåler maksimalt 100 [bar], som direkte påvirker hvor mye gas som kan brukes for pre-forbrenningen. Mengden av gassblandingen som det gamle tenningsystemet var i stand til antenne kan ikke økes vesentlig uten å nå den trykkgrensen.

Disse aspektene ble undersøkt i dette foreliggende arbeid ved å installere to typer antenningssystemer som har som mål å initiere en mer symmetrisk pre-forbrenning, samt å være i stand til å antenne uttynnede gassblandinger. Det konvensjonelle induktive tenningsystemet fra Motortech, med en dobbel tennplugg konfigurasjon, og et alternativt antenningssystem som bruker korona utladning laget av Øystein Smith og medstudenter på Omega verksted på Norges Tekniske-Naturvitenskaplige Universitet (NTNU).

Forsøket vi utført på den konvensjonelle tenning indikerte et høyere trykknivå og en hurtigere pre-forbrenning med dobbel tennplugg konfigurasjon sammenlignet med en enkelt tennplugg konfigurasjon, noe som kan redusere temperaturgradienten, men videre eksperimenter er nødvendig for å konkludere med dette problemet. Systemet viste en forbedret evne til å antenne magre blandinger, under forsøk hvor volumandelen av karbonmonoksid (CO) ble redusert når gass blande tanken ble ytterligere trykksatt med nitrogengass (N₂).

Antenningssystem med koronautladning har lovende egenskaper som en symmetrisk tenningskilde for å løse begge problemer beskrevet over. Utfordringen er å innføre spenningen inn i forbrenningskammeret uten å nå den dielektriske styrken av det isolerende materiale som omgir den ledende elektroden. Dette ville skape en lysbue mellom elektroden og det jordede forbrenningskammeret. De første forsøkene vi gjennomførte resulterte i gnist og ikke korona med de tre utviklede elektrodene under denne prosessen. Videre utvikling på elektrodene og et mer kontrollerbart signal for å styre korona driver er nødvendig for å få dette tenningsystemet til å fungere

Preface

This master thesis is written during summer 2016 and is my final proof of my academic pursuit for the degree Master of Science at the Norwegian University of Science and Technology (NTNU) in Trondheim. The thesis has been an integral part of my specialization in Marine Machinery and I will in the following like to thank all contributors for giving me the knowledge and guidance on this challenging process.

My initial academic supervisor, now Assistant Professor Per Risberg at KTH-Royal Institute of Technology in Stocholm, introduced me to the flourishing team-minded work being conducted on the CVCC at the machinery laboratory at the faculty of Marine Technology. His belief in me made me very eager to contribute to his team with a more practical approach within the scope of this present work.

Former PhD Candidate Maximilian Malin at NTNU, now pursuing his PhD degree and working as a research engineer in dual fuel combustion in TU Graz, needs to be highlighted for his positive spirit and his open door policy. He has contributed with his knowledge, and is one whom I have consulted whenever I have needed guidance.

All the very skilled people working on the laboratories at NTNU who have contributed to this present work. This work could not have been conducted without the help of Senior Engineer Frode Gran, Engineer Gunnar Bremset, Staff Engineer Kristian Minde, Senior Engineer Astrid Salvesen and other employees working at the machinery lab at the institute of Marine Technology.

Øystein Smith, and fellow students at the Omega Workshop, for designing and producing both the driver and the coil for the Corona Discharge Ignition System. Taking this task was bold, and demanding due to the workload on their daily life, not to mention the cascade of questions from me due to my lack of knowledge on this topic.


The friendly staff at Motortech and especially CEO Florian Virchow for taking interest in our application, for insuring us that the final order was according to our specifications.

PhD Candidate Vladimir Krivopolianskii has been by far the most important advisor. Without him around, none of this work would have been conducted.

Associate Professor Eilif Pedersen for taking over the responsibility as academic supervisor for me during the final and important period of this work.

My family for their enduring support, especially my always positive mother and father reminding me about “Hovedstolen”, my dear Guru Samantha Varner for her heroic effort of correcting this thesis, and last, but not least, my partner Kirsti for all the support in the world.

Trondheim, October 10, 2016


Peter Sommerseth Jaer

Contents

Abstract	iii
Sammendrag	v
Preface	vii
Contents	ix
List of Figures	xi
List of Tables	xiii
1 Introduction	15
1.1 Background and Motivation	16
1.2 Aim	18
1.3 Structure.....	19
2 Research Equipment and Pre-Combustion	21
2.1 Constant Volume Combustion Chamber	22
2.2 Capturing Techniques.....	24
2.3 Creating the thermodynamic condition inside the CVCC	26
2.4 Gas mixing room and filling procedure.....	27
2.5 Limiting Factor on the CVCC	29
2.6 Old Ignition System.....	30
3 Ignition Systems	31
3.1 Conventional Spark Ignition.....	32
3.1.1 Inductive Ignition system.....	33
3.1.2 Capacitive-Discharge Ignition Systems	34
3.2 Alternative ignition systems	35
3.2.1 Jet ignition.....	36
3.2.2 Laser Ignition	37
3.2.3 Corona Ignition	38
4 Design and Installation of Parts and New Equipment for the CVCC	43
4.1 Motortech- State of the Art Inductive Ignition System	44
4.1.1 Design and Manufacturing of M18 Rig Plugs for the CVCC.....	45
4.1.2 Out leaning Program	46
4.2 Corona Discharge Ignition System	49
4.2.1 Corona Discharge Ignition Driver	49
4.2.2 Corona Electrode- The Modified Spark Plug	52

4.2.3 Coil.....	55
4.2.4 Faraday Cage for the Coil	57
4.2.5 Final Set-up for the Corona Discharge Ignition System	58
5 Experiments and Results of the Ignition Systems	59
5.1 Motortech Ignition System	60
5.1.1 Test procedure.....	60
5.1.2 Results of MP104.....	61
5.2 Corona Discharge Ignition System.....	67
5.2.1 Test procedure.....	67
5.2.2 Result Test I- Modified Spark Plug I.....	68
5.2.3 Result Test II- Modified Spark Plug II	69
5.2.4 Result Test III- Insulated Steel Rod.....	71
6 Conclusion.....	73
6.1 Conclusion	74
6.1.1 Motortech Ignition System	74
6.1.2 Corona Discharge Ignition System	74
6.2 Suggestions for Further work	75
6.2.1 Motortech Ignition System	75
6.2.2 Corona Discharge Ignition System	76
References	77
Appendix	I

List of Figures

Figure 1: Operation Range for the Different Test Rigs [1]	16
Figure 2: Reactive Shot of Fuel Injected Into CVCC [3].....	17
Figure 3: Non-Reactive Shot of Fuel Injected into CVCC [3].....	17
Figure 4: Flame-front Propagating Inside CVCC [3].....	17
Figure 5: The Combustion Laboratory at MARINTEK and the CVCC Test Bench	22
Figure 6: Schematic Flow Plan of the Rig with Attached Sub-Systems [4]	23
Figure 7: Gas Bottles Inside the Gas Mixing Room	23
Figure 8: Direct Imaging Setup [4] and the Corresponding Image Result.....	24
Figure 9: Shadowgraph Principle [4]	25
Figure 10: Shadowgraph Setup [4].....	25
Figure 11: Schlieren Setup [4]	25
Figure 12: Combustion Rig Working Principle [4].....	26
Figure 13: Gas Mixing Arrangement [4].....	27
Figure 14: Typical Load Condition Curve [4]	29
Figure 15: Bosch Super Coil KW Red Used in the Old Ignition System on the Rig.....	30
Figure 16: Volt and Current Variation with Respect to Time [s] [7]	32
Figure 17: Arc and Glow Phase Respectively Illustrated	32
Figure 18: Schematic of an Inductive Ignition System	33
Figure 19: Schematic of Transistorized Coil Ignition	33
Figure 20: Schematic of a Capacitive-Discharge Ignition System	34
Figure 21: Exhaust Emission Related to Equivalence Ratio [7]	35
Figure 22: Minimum Ignition Energy for Varying Air-Fuel Ratios [7].....	35
Figure 23 : Early Design of Flame Jet Ignition Concept [7]	36
Figure 24: Jet Ignition Device Developed by Mahler [18]	36
Figure 25: Laser spark design by NETL	37
Figure 26: Schematics of Laser Induced Ignition with Spark Plug Protruding Design [24] ...	37
Figure 27: Discharge Regimes	38
Figure 28: Electrical Field Around Electrode Tip Producing Corona Region and Streamers .	39
Figure 29: Ionization Process Illustrated.....	40
Figure 30: Corona Streamers in Different Electrical Fields Due to Pressure Variation [31]...	40
Figure 31: Temperature Zones Relative to Distance from Electrode Tip [32]	41
Figure 32: Øystein Smith Delivers the Finished Driver.....	42
Figure 33: Schematics of The Conventional Ignition System from Motortech	44
Figure 34: Installation and Implementation of the System	44
Figure 35: The Conventional Ignition System Installed on the CVCC.....	45
Figure 36: Final Outcome of Rig Plug for M18 Spark Plugs.....	45
Figure 37: Volume Fraction of CO Depending on Added N ₂ to the GMB	48
Figure 38: Illustration of Corona Discharge Ignition System	49
Figure 39: The Corona Driver	49
Figure 40: Signal to the Driver for Output Control	50
Figure 41: Simple Circuit Presentation of the System ¹²	50
Figure 42: Tuning the Driver	51
Figure 43: Cutaway in a Spark Plug [7]	52

Figure 44: 3D Model of Spark Plug Made in Catia	53
Figure 45: First Modified Spark Plug	54
Figure 46: Position of Modified Spark Plug Tip inside the CVCC	54
Figure 47: Electrical Field Lines Around Conducting Wire and Coil	55
Figure 48: Illustration of Transformer Basic Construction	56
Figure 49: Omega Workshop Making the Coil	56
Figure 50: The Coil Made by Øystein Smith and Fellow Students at the Omega Workshop .	57
Figure 51: Electrical Field and Faraday Cage	57
Figure 52: 3D Model of Faraday Cage Made in Catia	58
Figure 53: The Coil Installed inside the Finished Faraday Cage	58
Figure 54: Illustration of CVCC and Spark Plug Positions	61
Figure 55: Images of Flame Front Propagating from Spark Plug Position 3 and 3/8	62
Figure 56: Pressure Development Inside CVCC for Point 1 and 2 for MP104	62
Figure 57: Images of Flame Front Propagating from Spark Plug Position 3/8 and 6	63
Figure 58: Pressure Development Inside CVCC for Point 3 and 4 MP104.....	63
Figure 59: Pressure Development Inside CVCC with Gradually Reduced CO Vol [%]	64
Figure 60: Out Leaning Process and Gas Composition	65
Figure 61: Pressure Development Under Similar Conditions for MP99 Versus MP104.....	66
Figure 62: Front Panel and Safety Buttons on the Driver	67
Figure 63: Detailed Picture of Scorched Insulating Tape After Test 1	68
Figure 64: Removing Internal Resistance Inside the Spark Plug	69
Figure 65: The 40 [cm] Machined Steel Rod with Pointy Tip and Terminal End Connector .	71
Figure 66: Test III Setup with the Electrode Protruding the CVCC	71
Figure 67: Visual Documenting Results from Test III.....	72
Figure 68: Illustrated Corona Discharge from the Tip of the Electrode	72
Figure 69: Illustration of Integrated Electrode in Rig Plug for Maximized Insulation.....	76

List of Tables

Table 1: Different Test Rigs with Operation Area	16
Table 2: Chemical Reactions with Excess Air after Combustion	26
Table 3: Gas Mixing Filling Process	28
Table 4: Lambda Classification Regarding Air Fuel Mixtures	46
Table 5: Gas Composition for Pre- Combustion	47
Table 6: Important Parameters and Boundary Conditions for the Test.....	61
Table 7: Conducted Points under MP104 regarding Vol [%] of CO and Spark Plug Position	61

Chapter 1

Introduction

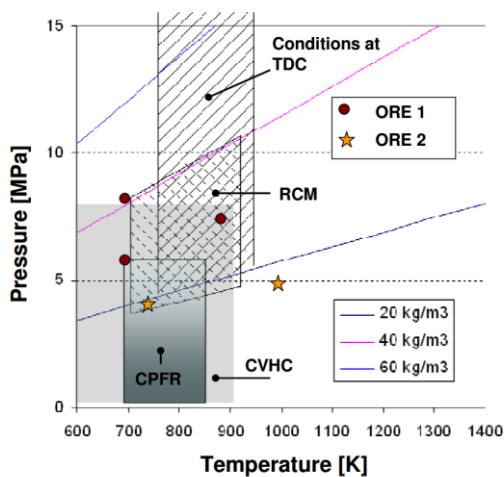
The following paragraphs outline the motivation for this work, the scope and wanted outcome and how the thesis is structured.

1.1 Background and Motivation

Combustion research is a key factor to further increase the knowledge on combustion processes and injection of fuel. These issues are greatly affected by new regulations, which are finally becoming stricter as decision makers see the correlation between different pollutions and the health and environmental issues related to them. Optimization of these processes for more efficient combustion and reduced emission levels, is strongly dependent on scientific experimentation and work in this field.

Research on combustion processes and injection has a small time domain, and is highly dependent on the thermodynamic state of the environment; pressure, temperature and other factors regarding composition of the fuel and geometry of the combustion chamber to mention some. To simulate the conditions that the fuel is subjected to inside of a cylinder, some test benches have been developed. Engine Combustion Network (ECN) is a network of different research centers each with their own research tools for combustion studies. The network determines how these studies can be compared, regardless of equipment, given that the boundary conditions are equal [1].

The *Table 1* below contains some research test rigs with some information, and *Figure 1* shows their operation range regarding temperature and pressure [2].



Test rig	Simulates	Acronym
Rapid Compression Machine	One compression stroke during a engine cycle	RCM
Constant Pressure Flow Rig	A single engine combustion chamber using additional flow into the rig to pressurize the rig	CPFR
Constant Volume Pressure Cell	A single engine combustion chamber using pre-combustion to pressurize the rig and to simulate the conditions at top dead center right before injection takes place	CVPC
Constant Volume Hot Cell	Increases the temperature with external heat elements.	CVHC
Optical Research Engine	These engines have optical access into the combustion chamber	ORE

Figure 1: Operation Range for the Different Test Rigs [1] Table 1: Different Test Rigs with Operation Area

The CVCC at the laboratory for combustion research at MARINTEK is a Constant Volume Pressure Cell (CVPC), see Table 1, and is used to conduct experiments on combustion and injection of fuel. Particularly reactive and non-reactive spray characteristics are studied while being injected into the chamber. Reactive sprays occur if the environment is suited for combustion, e.g. an oxidizer is present inside the pressurized and heated CVCC, while the non-reactive sprays are studied when the CVCC is either filled with the inert gas N₂ or without pre-combustion, see *Figure 2* and *Figure 3* respectively.

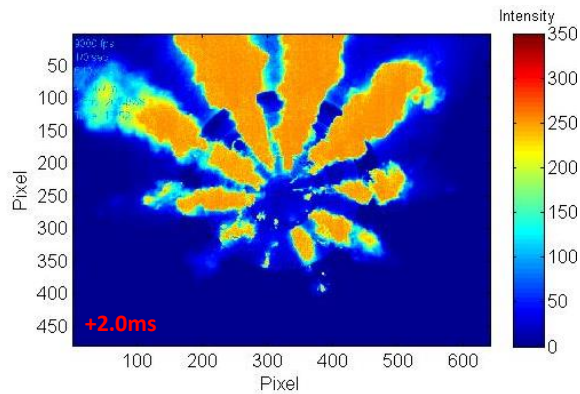


Figure 2: Reactive Shot of Fuel Injected Into CVCC [3]

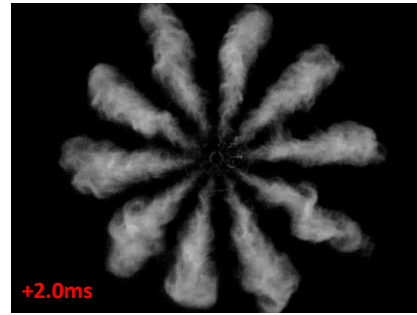


Figure 3: Non-Reactive Shot of Fuel Injected into CVCC [3]

The images above show both the reactive and a non-reactive results after experiments conducted on the CVCC. What we clearly see is a difference in the spray formation. Based on these images, a hypothesis is presented. This hypothesis suggests that the unsymmetrical combustion occurs due to an inhomogeneous temperature field inside the CVCC, which is due to unsymmetrical initiation of the pre-combustion. This is further explained, with the assumption of greater heat losses in the lower part of the CVCC to the surrounding area after pre-combustion, by looking at the flame front propagation in Figure 4. The pre-combustion is initiated by the spark plug positioned in the bottom of the CVCC. Here the flame front travels upwards, subjecting the surrounding chamber walls to an unequal and uneven amount of heat depending on the walls position in the vertical axis. The flame front propagation of CO is relatively slow, which subjects the lower part of the CVCC to a substantially longer period of heat loss compared to the upper part. Higher temperature results in better conditions for the composition of the gas used for pre-combustion.

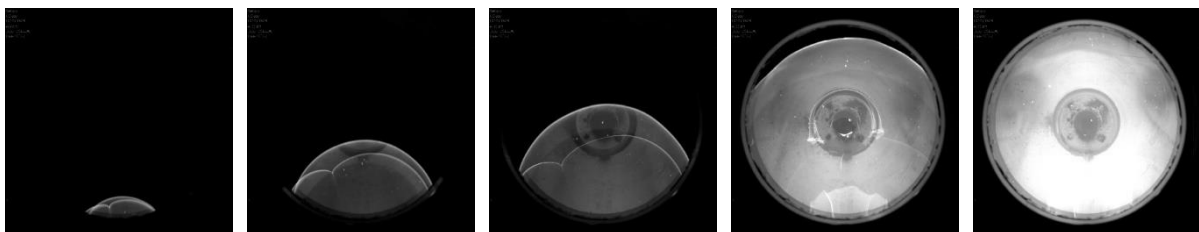


Figure 4: Flame-front Propagating Inside CVCC [3]

1.2 Aim

According to our postulated hypothesis, a more symmetrical initiated pre-combustion will decrease the temperature gradient, and hence improve the thermodynamic properties for the CVCC in terms of reproducibility. Spray investigation where the sprays differ depending on the temperature field minimizes the meaningful outcome of such test.

The aim for this thesis is to implement the conventional ignition system purchased from Motortech, and the more alternative and complicated Corona discharge ignition system made by Øystein Smith at the Omega Workshop. The Motortech system will be tested towards previous tests to investigate whether this ignition system improves the temperature field. The alternative ignition system with the Corona discharge needs more attention before testing can be initiated. My task is to find a method to introduce the high voltage into the CVCC. Design and test of an electrode which is capable of producing corona discharge streamers inside the CVCC.

We also want to conduct tests where these ignition systems are tested towards their capability to ignite leaner mixtures. That would allow us to increase the density inside the CVCC without overshooting the pressure that the CVCC can withstand and to improve the environment we are capable of simulating.

1.3 Structure

Chapter 1 has briefly outlined the problems related to the pre-combustion, the background for this present work, the postulated hypothesis, and how we want to improve these issues.

Chapter 2 presents the research equipment in the laboratory, describes the pre-combustion, and explains how the CVCC simulates the engine like conditions, including the imitating factors that we want to address with more powerful ignition methods and systems.

Chapter 3 gives a brief overview of the different ignition methods both conventional and more alternative methods. The Corona phenomena, fundamentals and some more detailed explanation are given in this chapter

Chapter 4 contains the design process and final outcome for the equipment we needed for both ignition systems. The chapter also presents the program, which was developed for the out leaning process.

Chapter 5 is where the conducted experiments and the results from these tests are presented and the new actions are discussed.

Chapter 6 presents the conclusions we are able to draw based on the results. It also contains my suggestions for further work regarding the scope for this present work.

Chapter 2

Research Equipment and Pre-Combustion

This chapter describes the laboratory with its research equipment in context to this master thesis. First, the test bench with general dimensions and properties will be described and then, the experimental process and principles with its limiting factors.

2.1 Constant Volume Combustion Chamber

The CVCC is located at the combustion laboratory at MARINTEK, see *Figure 5*. The whole purpose for this CVCC is to be able to experiment with suitable research tools with a high degree of reproducibility when investigating the combustion properties, process and injection of different fuels.



Figure 5: The Combustion Laboratory at MARINTEK and the CVCC Test Bench

The current CVCC is designed for a maximum pressure inside of the chamber of 100 [bar] and a maximum temperature of 1800 [K]. This high pressure and high temperature allows us to simulate the conditions of an engine.

The CVCC has a cylindrical shape with a diameter of 250 [mm] and inner width of 100 [mm] giving it a volume of around 5 [dm³]. Optical access is obtained by two quartz glass on each side with a diameter of 150 [mm]. *Figure 6* shows the schematic of the combustion rig and the subsystems and equipment connected to it. The removable rig plugs provide the necessary access to the rig and the possibility of attaching different arrangements and instrumentation to the CVCC. Currently connected is a common rail fuel injection system with a maximum pressure of 1800 [bar], a spark plug (to initiate the pre-combustion – explained in Chapter 2.3), air and gas inlet valves, and an exhaust outlet valve. The newly installed fan provides a satisfying mixture of the gas and creates a homogeneous distribution inside the rig. It can also simulate turbulence while the fuel is injected besides that it improves the temperature field as David Koch concluded in his thesis [3]. A Piezo electric pressure sensor records the data and is used for further analysis. The camera used is a Photron Fastcam-APX-RS, a high-speed camera with a maximum of 250,000 frames per second and allows us to use different image techniques like Schlieren and shadowgraph.

Every subsystem and equipment is controlled from the control room with aid of LabView PC and proportional integral derivative controller (PID controller). The mixing of the gas, which will be explained later in *chapter 2.4*, has to be mixed manually as of today in a well-ventilated room see *Figure 7*, but the filling of the CVCC of the mixed gas is controlled from the control room.

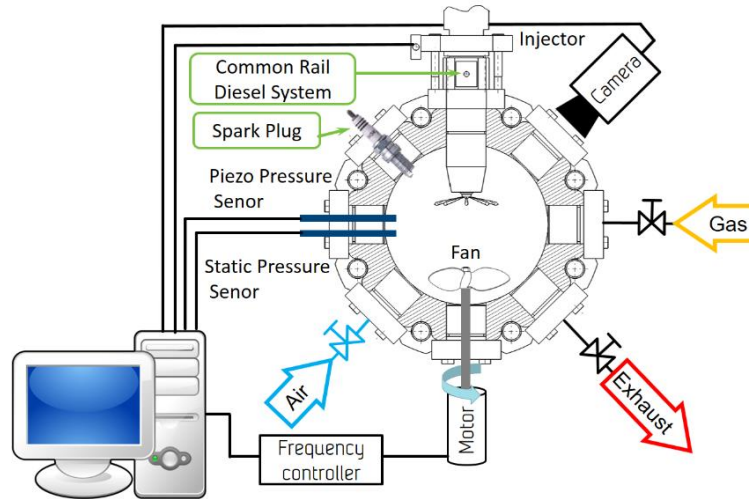


Figure 6: Schematic Flow Plan of the Rig with Attached Sub-Systems [4]



Figure 7: Gas Bottles Inside the Gas Mixing Room

2.2 Capturing Techniques

The laboratory is equipped with a high-speed camera as previously mentioned. The camera and the different optical arrangements let us visualize the combustion process inside of the chamber. Direct imaging, shadowgraph, and schlieren image techniques are examples of methods used to capture the chemical reaction with different outcome. Direct imaging is ordinary photos used to capture the radiation intensity. The setup with optical arrangement is the simplest of the three techniques, see *Figure 8* [4]. The direct image technique was the only experimental setup used to visualize the pre-combustion experiment conducted in context to present work. The first image where two flame fronts are propagating towards each other was captured with direct image and can be seen in *Figure 8*.

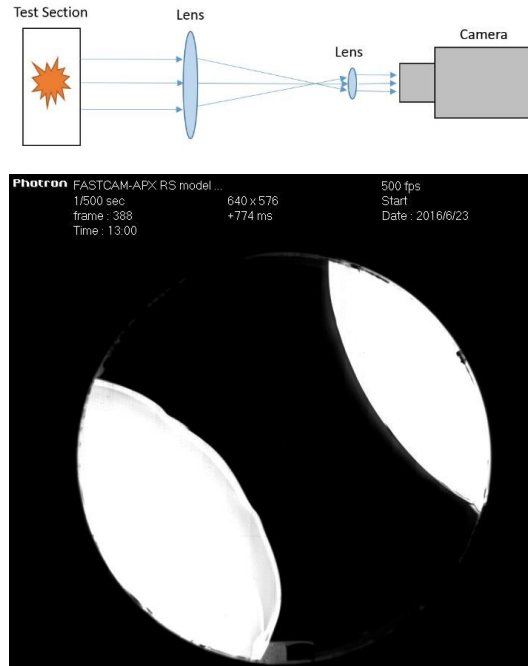


Figure 8: Direct Imaging Setup [4] and the Corresponding Image Result.

Shadowgraph is a technique that shows the density gradient, which is a result of refraction of light depending on the speed of the light through the medium it travels. This correlation is called Snell's law, *Eq. (2.1)*. The defraction index n of the medium can be found together with the Gladstone-Dale formula, *Eq. (2.2)*. This formula gives the relation between refraction index n and density ρ and makes it possible to visualize the density variation inside the CVCC. k is the Gladstone-Dale constant.

$$\frac{\sin(\alpha_1)}{\sin(\alpha_2)} = \frac{n_1}{n_2}, \quad n = \frac{C_{vacuum}}{C_{Medium}} \quad (2.1)$$

$$n - 1 = k\rho \quad (2.2)$$

Figure 9 shows the relation between the deflected beams of light and the image. Where the light has been deflected, the image will appear as a darker area and the areas where several light rays coincide will have more light. The higher densities can be seen as darker areas with a brighter field next to it [5]. Density is temperature dependent and is therefore an important method to analyze the combustion process.

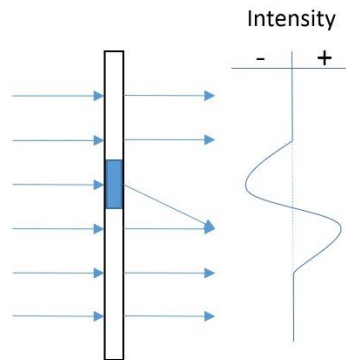


Figure 9: Shadowgraph Principle [4]

The optical arrangement is relative to direct image and is more complicated to set up as is illustrated in *Figure 10*.

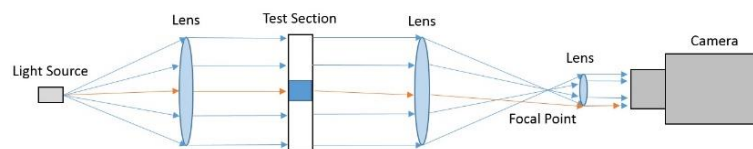


Figure 10: Shadowgraph Setup [4]

Schlieren image technique is the last method we can conduct with the optical arrangement in the engine laboratory. This method is almost identical to shadowgraph with the only difference being a barber knife-edge blocking light rays, see *Figure 11*. Depending on the position and the geometry of the edge used, different rays will be blocked. This creates different images since the density field that is captured is the density variation perpendicular to the knife-edge. This is a very suitable method to obtain a more detailed image of the density field.

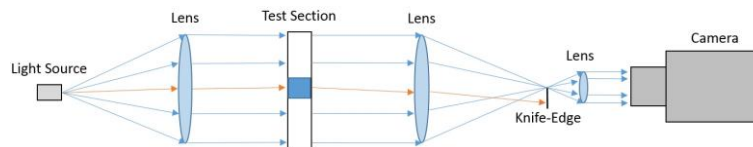


Figure 11: Schlieren Setup [4]

2.3 Creating the thermodynamic condition inside the CVCC

The CVCC has to pressurize and heat up the environment to get the conditions where auto-ignition of diesel fuel is possible. This is accomplished by igniting a gas mixture inside the CVCC. This process is called pre-combustion and is a chemical heating process which utilizes a lean gas mixture containing O_2 , CO and N_2 . This gas composition is a result of the assumption of complete combustion and that the composition has to have satisfying O_2 levels before the main combustion. *Figure 12* shows the working principle of the pre-combustion. The CVCC is filled to a desired pressure level (in this case 10 [bar]) and the spark ignites the mixture. This chemical reaction increases the pressure (blue line) and temperature (red line) quite rapidly. Both parameters are too high to simulate actual engine condition just after the ignition, resulting in a short period where the CVCC is cooled down naturally by means of heat loss. The main combustion is set to commence at a certain pressure/temperature level, which triggers the injection of the fuel.

By adjusting the gas composition for the pre-combustion, the experiment conducted in the CVCC, in terms of what we are investigating, can be changed. Both reactive sprays with a volume fraction in excess of 21 [%] O_2 or non-reactive sprays and Exhaust Gas Recirculation (EGR) where less than 21 [%] O_2 is present inside the CVCC is possible to achieve, see *Eq (2.3-2.6)*.

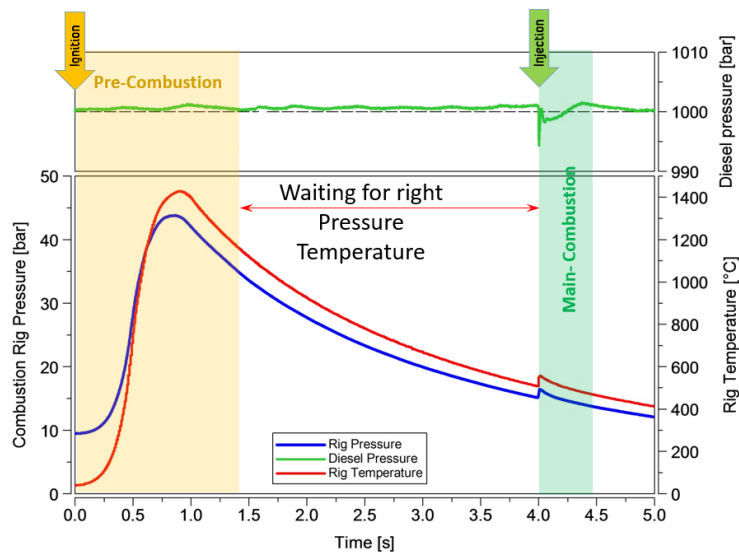


Figure 12: Combustion Rig Working Principle [4]

$X_1O_2 + X_2N_2 + X_3CO \rightarrow Z_1O_2 + Z_2N_2 + Z_3CO_2$	Complete reaction	(2.3)
$2X_1 + X_3 \rightarrow Z_1O_2 + 2Z_3$	For Oxygen	(2.4)
$X_2 \rightarrow Z_2$	For Nitrogen	(2.5)
$X_3 \rightarrow Z_3$	For Carbon	(2.6)

Table 2: Chemical Reactions with Excess Air after Combustion

2.4 Gas mixing room and filling procedure

The gas-mixing laboratory is located beside the engine laboratory. This room contains each of the components used in the gas mixture in separate bottles, see *Figure 13*. The filling process is manually executed. Each of the three species is filled up to a specific pressure level, depending on the desired composition of the Gas Mixing Bottle (GMB). The GMB has a maximum rated pressure of 300 [bar], but due to safety precautions the bottle is only filled up to 40 [bar]. This is because the bottle is filled with an ignitable mixture that may cause backfires and flashback. By having set this limitation, the bottle will, in a worst-case scenario, withstand the unwanted situation where the whole content ignites.

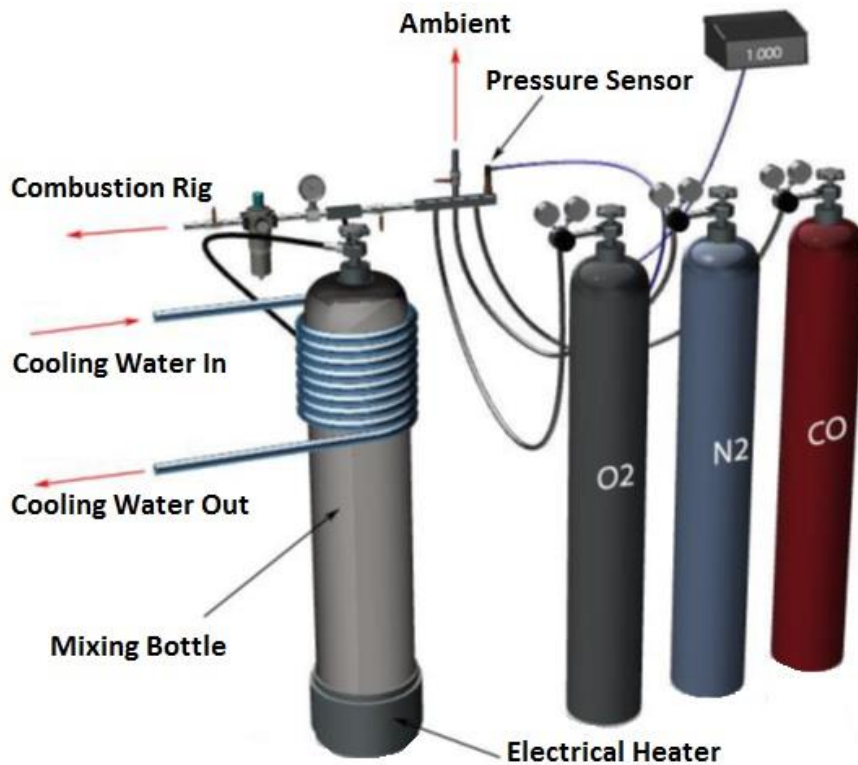


Figure 13: Gas Mixing Arrangement [4]

The gas composition is calculated in a backwards manner, stating first the wanted O_2 level after the pre-combustion. Then a minimum amount of the fuel CO has to be added so that the mixture is ignitable and able to reach a satisfying level in terms of pressure and temperature inside the CVCC. N_2 is an inert gas and is only used to achieve desired volume fraction in the mixed gas. Eq. (2.7-2.10) is used to calculate the partial pressure of each component. Every component “i” has a known molar mass (M_i) and since the volume of the GMB is known, we can use the ideal gas law and fill the desired amount of each component. Each of the partial pressures of the component is summarized in *Table 3*. Note the filling order where O_2 is added last to the mixture. This ensures the safest filling due to the lean composition under the filling process since leaner mixtures are harder to ignite. After the filling has been done according to the process, the mixing bottle has to mix to ensure that the mixture is as homogenous as possible. This is accomplished by a heating element attached to the bottom and a cooling element

attached on the top of the gas-mixing bottle. After the mixture has cooled down to a satisfying temperature level, the gas is ready to flow from the GMB to the CVCC. The filling pressure of 10 [bar] gives approximately 30 fillings of the CVCC. Previous experiments have shown poor ignition properties if the mixture is not used immediately after mixing. This is due to how the gases will distribute into layers depending on the density of the components, and a slow reaction between the components resulting in deviation of the homogenous gas mixture.

$$P_i = r_i \times P_{GMB} \quad (2.7)$$

$$P_i V_{GMB} = m_i R_i T \quad (2.8)$$

$$R_i = \frac{R_m}{M_i}, R_m = 8,314 [kJ/KmolK] \quad (2.9)$$

$$m_i = n_i \times M_i \quad (2.10)$$

Gas	Partial Pressure [bar]	Cumulative Pressure [bar]
Air	1	1
Nitrogen	9.2	10.2
Carbon monoxide	17.9	28.1
Oxygen	11.9	40

Table 3: Gas Mixing Filling Process

2.5 Limiting Factor on the CVCC

The most important and governing factor in the CVCC is the maximum pressure allowance. The peak pressure occurs during the pre-combustion, and is directly linked to the amount of energy we introduce to the CVCC in terms of composition of the gas mixture. Increased CO level increases the energy content and hence increases the peak pressure. The conditions we want to simulate inside the CVCC depend on the density. Being able to ignite leaner mixtures (reduced volume fraction of CO) that lowers the peak pressures, is one of the objectives in this present work if time allows. *Figure 14* illustrates the general relationship for Break Mean Effective Pressure (BMEP) and density in the cylinder for a medium speed one stage turbocharged CI engine [4]. This general load condition curve illustrates that the conditions that we are capable of simulating in the CVCC is currently not satisfactory since the Peak Cylinder Pressure (PCP) is too low. See also the operation range for different test rigs in *Figure 1*.

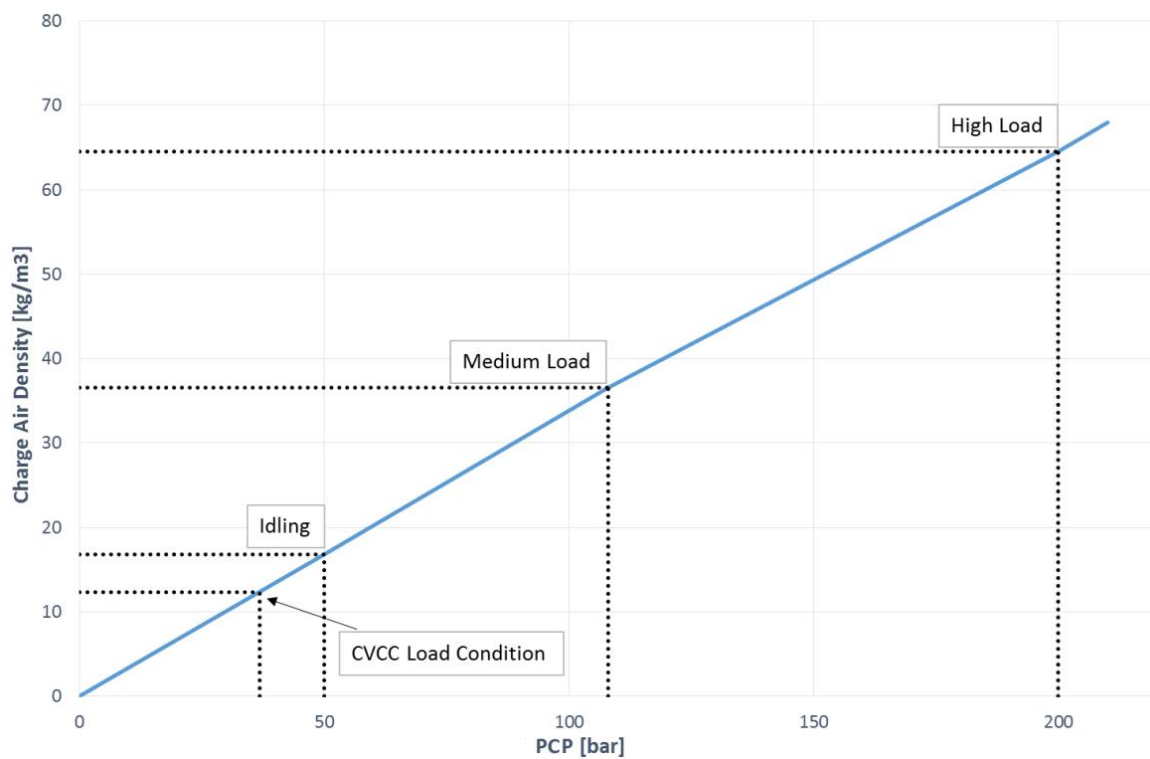


Figure 14: Typical Load Condition Curve [4]

2.6 Old Ignition System

This ignition system was made in-house from an old ignition system from a car and was controlled by an ignition controller connected to the Labview PC with unknown origin. The voltage was transformed to approximately 26,5 [KW] [6]. Information of energy delivered by this ignition system is not known, but the literature gives values ranging from 50 [mJ] and below for this type of ignition systems [7]. *Figure 15* shows the coil used and the setup on the CVCC.

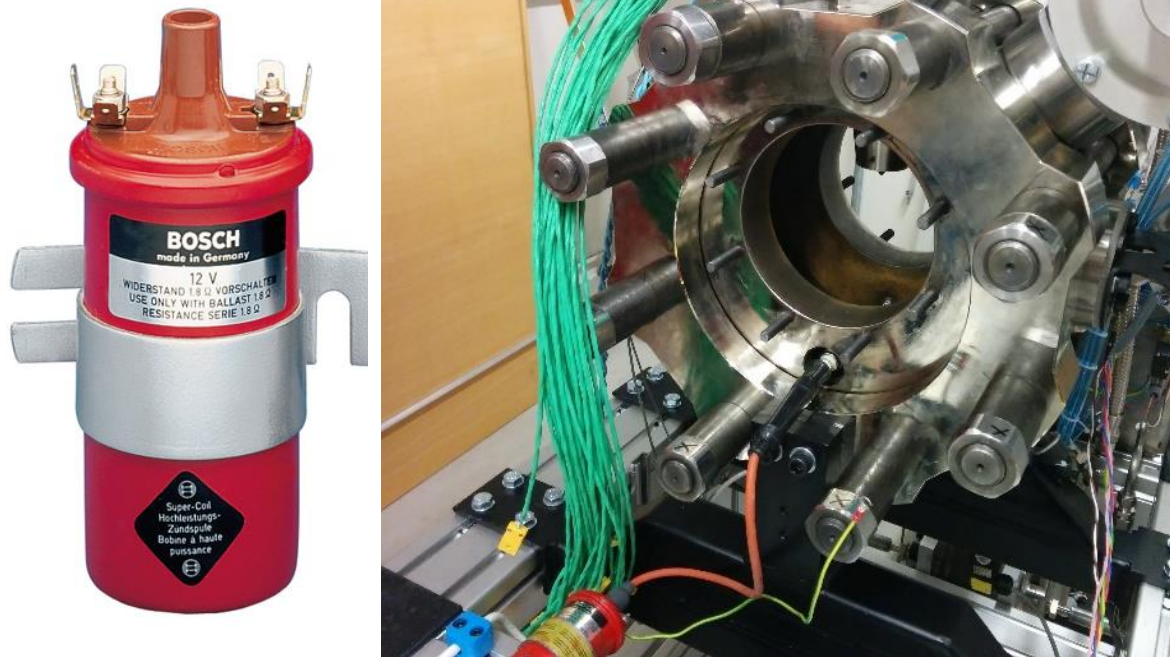


Figure 15: Bosch Super Coil KW Red Used in the Old Ignition System on the Rig¹

¹ http://www.boschcarservice.pt/boaa-pt/Product.jsp?prod_id=70&ccat_id=32&language=en-GB&publication=1

Chapter 3

Ignition Systems

In this chapter I will present a brief overview of existing ignition systems. The alternative ignition method with Corona discharge will be explained in terms of basic theory and fundamentals and why this interesting discharge is promising as an ignition source for our application.

3.1 Conventional Spark Ignition

The spark ignition system is a vital system in the spark ignited engines, and has been so since its introduction in the late 19th century [8]. The purpose of the spark ignition system is to deliver the needed energy to a spark plug at a precise time so the air-fuel mixture ignites. The spark discharge consists of three different phases as illustrated in

Figure 17-not showing the breakdown phase. Voltage between the electrodes is increased until the breakdown of the intervening mixture occurs. Then ionizing streamers propagate towards the ground electrode and create a conductive channel. This discharge stage is called the breakdown phase and is followed by the arc phase. This phase is characterized by an increased cylindrical plasma around the electrode gap, as illustrated in

Figure 17. Due to heat conduction, diffusion and chemical reactions in the fuel-air mixture a propagating flame will develop if the ignition is successful. Depending on the system a glow phase can succeed the arc phase. The energy stored in the ignition storage device will dump the energy into the discharge circuit. The time domain for each phase and the delivered energy for each phase can be seen in *Figure 16*.

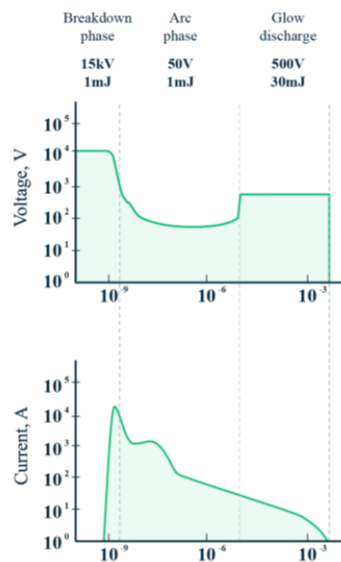


Figure 16: Volt and Current Variation with Respect to Time [s] [7]²

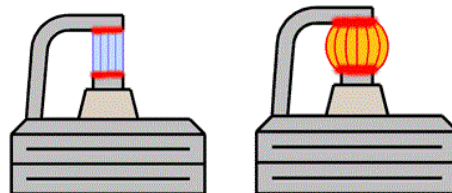


Figure 17: Arc and Glow Phase Respectively Illustrated³

² Modified with Adobe® for increased readability

³ http://www.daytona-twintec.com/tech_ignition.html

3.1.1 Inductive Ignition system

This common ignition system uses a coil to transform the voltage. The basic principle of a coil transformation is a current that generates an electromagnetic field when the primary circuit is closed (Breaker contact points), see *Figure 18*. When the contact breaker opens the circuit, the flow of current is interrupted and results in a decay of magnetic flux, which induces a voltage in both the primary and the secondary circuit of the coil. Due to a higher number of windings in the secondary circuit, the voltage will be transformed relative to the relation between the windings in the two circuits in the coil. The high voltage is then transferred to the spark plug through the distributor and high tension leads [7].

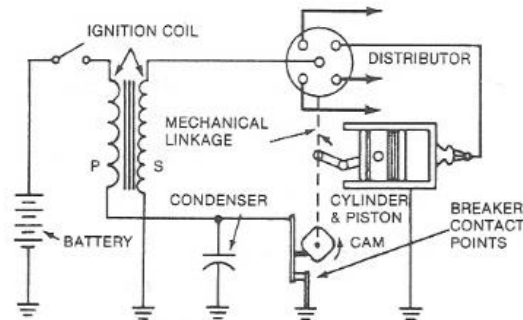


Figure 18: Schematic of an Inductive Ignition System⁴

Over the years, this system has transformed into a more complex system to decrease the maintenance and to increase the energy during the discharge phase. *Figure 19* shows the schematics for the high-energy electronic-ignition system also called Transistorized Coil ignition. The principle is still the same, but instead of the mechanical contact breaker, a magnetic pulse generating system is used. This system is based on the variation of a magnetic field produced by a gear-shaped iron rotor, with the number of teeth as cylinders, spinning around a stationary pole. These generated electrical pulses are then sent to the electrical control unit (ECU). The ECU then switches on and off the flow of current in the primary circuit to induce the high voltage on the secondary circuit.

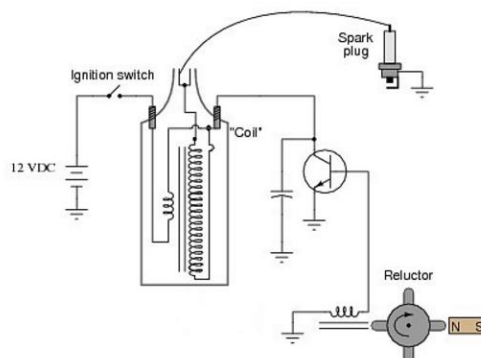


Figure 19: Schematic of Transistorized Coil Ignition⁵

⁴ <http://www.electroschematics.com/tag/automobile/>

⁵ <http://www.allaboutcircuits.com/>

3.1.2 Capacitive-Discharge Ignition Systems

This ignition system uses a capacitor instead of the coil to store the ignition energy. The exciter coil, see *Figure 20*, induces an AC voltage where only the positive voltage opens the flow through the diode and charges the capacitor [9]. When the silicon controlled rectifier (SCR) or thyristor is triggered by the voltage generated by the pulse rotor, the stored energy in the capacitor flows through the SCR and the ignition coil transforms up the primary voltage and a high voltage is applied to the spark plug.

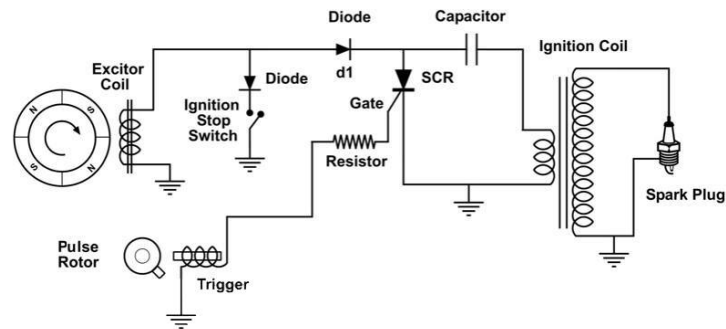


Figure 20: Schematic of a Capacitive-Discharge Ignition System⁶

⁶ <http://www.wiringdiagrams21.com/>

3.2 Alternative ignition systems

There have been numerous prosperous ignition systems that have been proposed and examined [7, 10-12]. Some of these suggested improvements have been on the design of the spark plug, the numbers of spark plugs, the spark duration, the energy delivered and the other more intricate systems like the flame-jet and plasma jet, not to mention the corona discharge and laser ignition systems. All of these ignition systems have a common goal and that is to extend the lean limit. This increasingly diluted air-fuel mixture has a promising concept to increase the thermal efficiency and decrease the exhaust emission in spark ignited engines see *Figure 21* **Feil! Fant ikke referansekinden.**, but the drawbacks like reduction of power output and slower flame propagation are a great challenge [13]. Only by overcoming these challenges can we reach the full potential of lean combustion [14]. Increasing the ignition voltage allows ignition of high charged mixture resulting in increased power output, but also an unfavorable increase of erosion on the electrodes. Increasing the flame speed is done by either enhancing the cylinder turbulence [15] for flame kernel development or minimizing the flame travel distance by the use of multiple spark plugs [16], or by optimizing the ignition point inside the combustion. We will therefor in the following present some ignition systems which to some extent enhance the ignition capability of lean limit ignition.

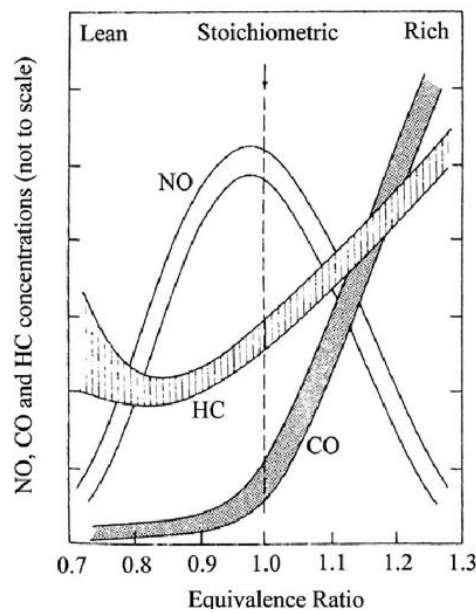


Figure 21: Exhaust Emission Related to Equivalence Ratio [7]

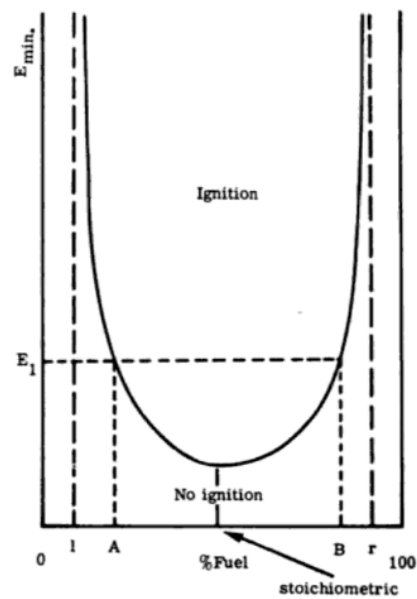


Figure 22: Minimum Ignition Energy for Varying Air-Fuel Ratios [7]

3.2.1 Jet ignition

Jet ignition is most commonly referred to as flame jet or plasma jet, depending on the design and behavior of ignition. The flame-jet ignition system is mainly a relocation of the spark plug into a pre-chamber with orifices connected to the top of the cylinder, see *Figure 23*. The cavity where the fuel-air mixture is ignited by a spark raises both the pressure and temperature. This forces the very turbulent burning jets into the main chamber like a torch where it initiates the combustion of the unburned mixture. By utilizing a cavity and a number of orifices or nozzles, the spherical flame kernel around the spark plug is transformed in a number of flame jets into the main chamber so the initiation of the combustion starts at several locations.

The Plasma Jet ignition has the advantage of sending out high temperature plasma into the main combustion chamber by discharging a substantially higher energy level (compared to inductive ignition) by the use of a capacitor. This is achieved by confining the electrode in an enclosed cavity with an orifice to the combustion chamber. The pressure and temperature will increase so rapidly inside the small cavity around the electrode, so that a supersonic jet of plasma flow is generated and introduced into the main chamber. The ignition of the gas-mixture is then initiated as a turbulent flame compared the flame propagation from a conventional ignition system which is more laminar.

Depending on the complexity of design, these systems have shown improved ignition parameters compared to common ignition but have an inconsistent effect on the exhaust gas emissions, particularly on the increased NO_x emission due to an increased combustion temperature [10]. Plasma jet ignition and pre-chamber design have become more intricate and compact over the years as *Figure 24* illustrates. The combustion duration has been further shortened with the introduction of hydrogen. This has increased combustion capability and lowered the equivalence ratio [17].

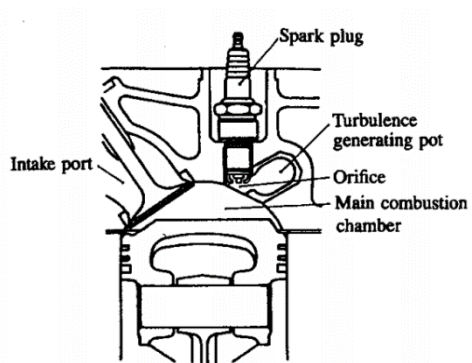


Figure 23 : Early Design of Flame Jet Ignition Concept [7]

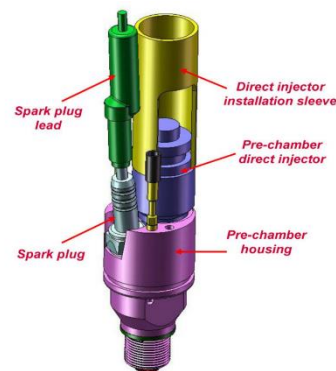


Figure 24: Jet Ignition Device Developed by Mahler [18]

3.2.2 Laser Ignition

Ignition with laser induced optical breakdown dates back to 1962 [19]. This method initiates the combustion sequence by the stimuli of a laser light source. Laser ignition is divided into four categories [20] depending on the method and is as follows:

- I) Thermal Ignition
- II) Photochemical Ignition
- III) Resonant Breakdown
- IV) Spark Ignition

Thermal Ignition occurs when the gas molecules absorb the laser energy which increases the kinetic energy. This energy absorption breaks the bonds in the molecules and lead to chemical reactions. In Photochemical Ignition, highly reactive radical is produced in the air-fuel mixture when it is targeted by the laser-photons. These photons break up the molecules and if the rate that the radicals are produced is greater than the rate of recombination, then it will lead to combustion. With Resonant Breakdown, the initial process is similar to Photochemical Ignition e.g. photo dissociation of some molecules. This dissociation will then ionize some atoms, which again will result in a number of free electrons. The electrons will be excited further by the laser energy until plasma is created. The final Spark Ignition method is initiated by the laser beam, which ionizes some of the gas molecules. The free electrons will then increase their kinetic energy and collide into other molecules and initiate a breakdown in the focal area of the laser via electron cascade growth.

All of the above mentioned methods have been investigated and have been reported to increase ignition capabilities [11, 12, 20-23]. The laser technology has also a key feature e.g. ignition monitoring. This together with arbitrary positioning of the ignition plasma and reduced emission in terms of NO_x makes the laser induced ignition promising. The overall price, size and challenges with optical access to the chamber make it more complex to put in commercialized engines at present moment. The *figures* below show a laser spark plug design by *National Energy Technology Laboratory (NETL)* and the schematics of this system



Figure 25: Laser spark design by NETL⁷

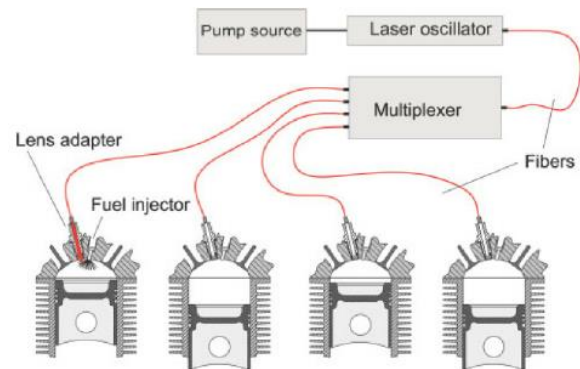


Figure 26: Schematics of Laser Induced Ignition with Spark Plug Protruding Design [24]

3.2.3 Corona Ignition

This chapter describes the corona discharge, and has been prioritized in this present work, since this ignition method is currently under development as a new alternative way of igniting air-fuel mixtures in spark ignited engines and since this ignition method was chosen as an alternative ignition system for CVCC at the combustion laboratory for present work.

3.2.3.1 Corona- Shown by Classification of Electrical Discharge Regimes

Different gas discharge is illustrated in *Figure 27*. This relationship between voltage and current is found for two electrodes separated with a gas inside a tube and shows different discharge regimes [25, 26]:

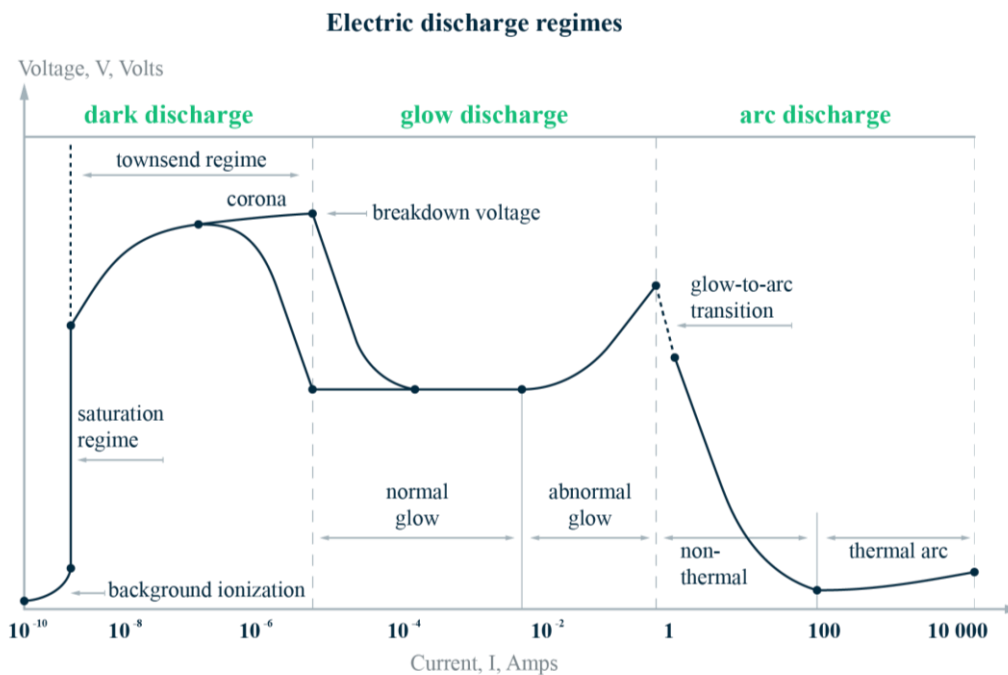


Figure 27: Discharge Regimes⁸

Non-self-sustained discharge: This discharge occurs before dark discharge and requires an additional ion source like cosmic radiation, photoionization, or thermionic. The generated charged carriers are accelerated towards the electrodes and the portion that reaches the electrode increases by increased voltage level, while some will recombine with other particles before reaching the electrodes.

Dark discharge: If the voltage is sufficiently high, electrons will ionize gas molecules due to impact ionization. This process will knock out more free electrons, which will be accelerated by the electrical field between the electrodes. If the number of free electrons from the ionized gas molecules is higher than the electrons being recombined, an avalanche of electrons will be produced. This process will be supported by two additional processes. One is caused by

⁸ http://www.glow-discharge.com/?Physical_background:Glow_Discharges:Discharge_Regimes and modified in Adobe®

accelerated positive ions towards the negatively charged electrode. These accelerated ions will knock out even more electrons on their way. The other process involves electrons that do not knock out other electrons from the gas molecules but excite them, so that they emit photons. These emitted photons will result in further ionization of the gas molecules.

Corona: Corona discharge occurs if the fluid around an electrically energized conductor becomes ionized. This ionization leads to positively or negatively charged particles (ions) near the conductor, due to the electromagnetic field. These particles will then find a path out of the conducting area and neutralize with other particles of opposite charge. The result is a glowing coverage around the conductor. At some distance from the conductor the glowing stops. This is due to the decrease in the electrical field where the ionization of the molecules stops.

Glow discharge: Increased current will transform the dark discharge into a glow discharge. This increased voltage will energize the electrodes to such an extent that it excites the gas molecule so they emit light. This will be seen as brighter glow

Arc discharge: This discharge will occur if the voltage overcomes the threshold voltage for complete breakdown and will result in a conductive channel between the electrodes. If the power source is capable of delivering sufficient energy the discharge will continue as an arc, if not it is characterized as a spark discharge.

3.2.3.2 Fundamentals and Basics of Corona Discharge

The corona discharge is a high voltage/low current discharge and is caused by the ionization of gas molecules generated by an inhomogeneous and strong electrical field [27]. Since the corona discharge is a pre-breakdown phenomenon, that only manifests itself in relatively small corona regions around geometrically charged objects where the free electrons from the ionized gas do not make a conducting channel between the electrodes [28]. The streamers will propagate out towards the region with opposing charge, see *Figure 28*.

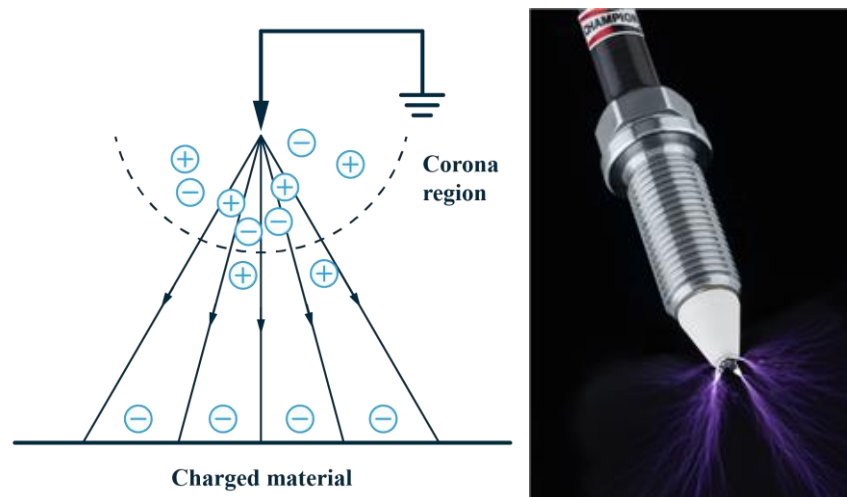


Figure 28: Electrical Field Around Electrode Tip Producing Corona Region⁹ and Streamers¹⁰

⁹ http://www.glow-discharge.com/?Physical_background:Glow_Discharges:Discharge_Regimes and Modified in Adobe®

¹⁰ <http://www.federalmogul.com/en-US/OE/Products/Pages/Product-Details.aspx?CategoryId=15&SubCategoryId=21&ProductId=224>

The corona phenomena is only possible if the magnetic field energizes the electrons sufficiently to start the ionization process of the gas molecules, when the dielectric strength of the gas is reached [29]. The electrode-far area where the electrical field is less, shields the ground potential and prevents dielectric breakdown or arcing to grounded objects [30]. The field intensity depends on several factors and is possible to calculate with the use of Peeks empirical equation, see Eq. (3.1)

$$E_p = 31\delta \left(1 + \frac{0,308}{\sqrt{\delta r}} \right) \tag{3.1}$$

δ corresponds to the relationship between air pressure and standard atmospheric pressure of 101,325 [kPa], while r to the radius of the electrode tip. This empirical formula gives the minimum field strength that will initiate the ionization process, see Figure 29

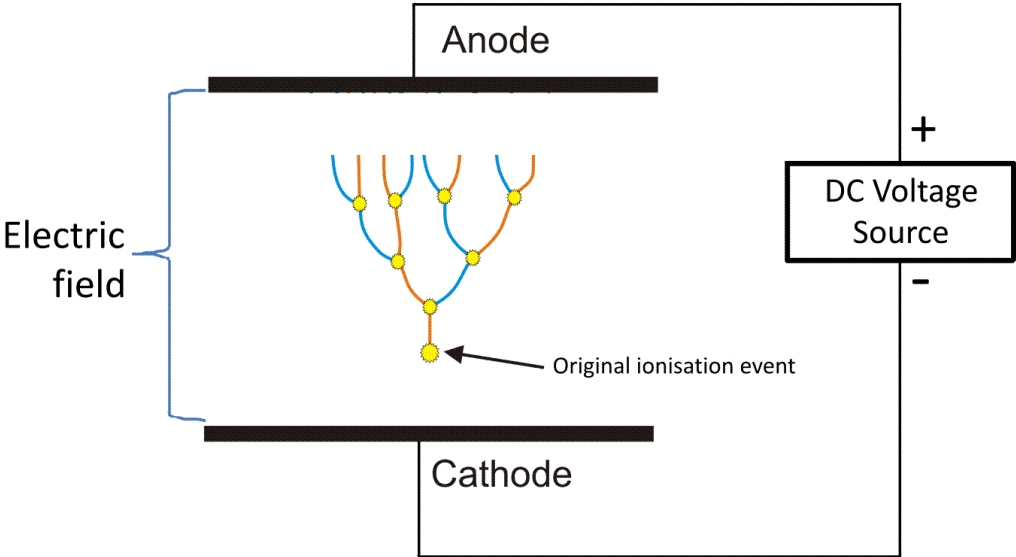


Figure 29: Ionization Process Illustrated¹¹

The equation states that increased air pressure will increase the minimum field strength, and this increased pressure gives shorter corona streamers as Figure 30 illustrates.



Figure 30: Corona Streamers in Different Electrical Fields Due to Pressure Variation [31].

¹¹ http://www.glow-discharge.com/?Physical_background:Glow_Discharges:Discharge_Regimes

If the voltage applied to the electrodes is increased after corona first appear, the brightness and intensity of the corona will increase and go from light almost barely visible dark discharge covering one of the electrodes to intense and glowing discharge. When the breakdown voltage is reached for the medium between the electrodes, an arc will develop immediately and form a conducting channel.

Corona can be quite similar to lightning in appearance and sonically, corona produce a crackling noise similar to thunder and has long branches that spreads outward. However, there is no conducting channel between the electrodes where corona occurs, so there is not a lot of heat generation as there is under lightning. The gas surrounding the electrodes can be divided into two zones, the area around the electrode tip which has the highest temperature (HT) and then decreases drastically towards lower temperature (LT) as the distance from the electrode increases, see *Figure 31* These images show the corresponding temperature for a setup where a point to plane gap with 13 [mm] gap length is used with a charge stored in a capacitor of 860 [pF].

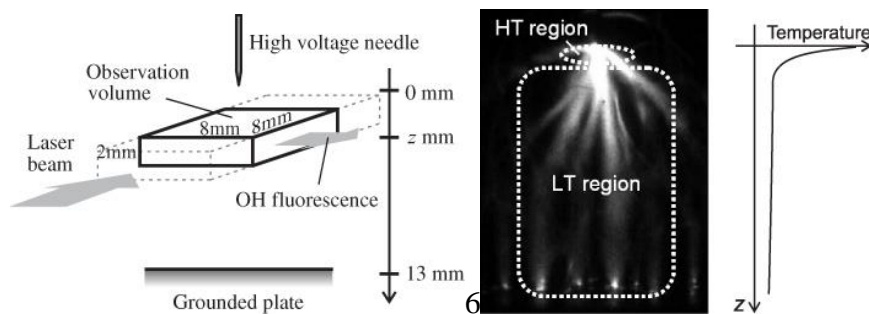


Figure 31: Temperature Zones Relative to Distance from Electrode Tip [32]

Another phenomenon which occurs during this discharge is corona wind [32]. This wind is generated by the ions, which are repelled by the electrode that has the opposite polarity as the ionized gas molecules. This repelling of the ionized gas molecules acts as a pushing force and results in a movement of the surrounding air. The corona wind has been reported as high as 7-10 [m/s] in the literature [33] and is stated as a beneficial contributor to turbulence and flame front propagation [34].

3.2.3.3 Generating Corona

Corona discharge has been investigated for many years and for different applications, and two main methods have emerged to produce corona: One using direct current (DC) at a high voltage and the other method involves the use of radio frequency (RF), which is generated by a resonant circuitry. The method which has been subjected to a lot of progress, according to literature [35-37], is the RF corona discharge also commonly referred to as a Tesla Transformer.

This type of resonant circuitry system was built by Øystein Smith and fellow students at the Omega Workshop for this present work as the alternative ignition method, see *Figure 32*. The architecture of this corona driver will not be discussed nor presented further in this work, but technical documentation as a preliminary user-guide from Omega is added in the appendix A.1.

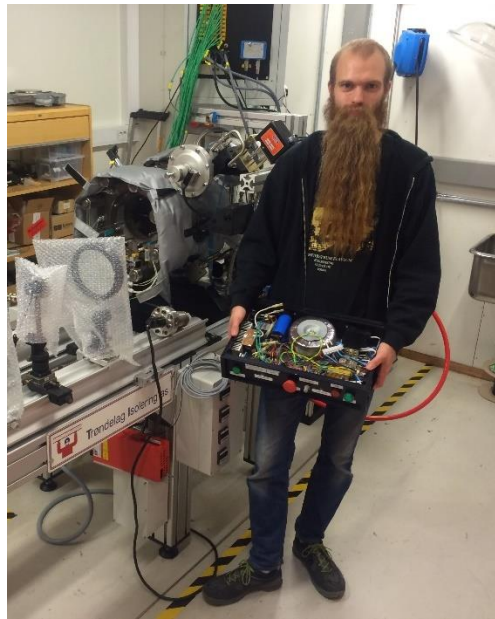


Figure 32: Øystein Smith Delivers the Finished Driver

3.2.3.4 Favorable Properties as Ignition Source

Corona discharge, with its high voltage and low current, initiates the chemical reactions without the need of overcoming the dielectric breakdown, resulting in more efficient ignition with less ignition energy [34]. The streamers spread from the pointy electrode and outwards and hence ignites a larger volume. Depending on the geometry of the electrode this area can be many orders of magnitude larger than in a traditional inductive spark plug [38]. This has the beneficial result of statistically igniting the fuel-air mixtures faster and more robustly due to increased number of radicals, e.g. ions. This is reported as one important promoter for a more complete combustion which lowers the emission of hydrocarbons (HC) and carbon monoxide (CO) [38]

This ignition method has also beneficial impact on the emission, where the literature is currently showing a huge decrease in NO_x emission with the use of Exhaust gas recycling (EGR) [38]. This is possible since corona ignition substantially stabilizes the combustion with high EGR rates. Pressure rise is also faster and the increased ignition area is possibly the promoter for a more complete combustion process

Chapter 4

Design and Installation of Parts and New Equipment for the CVCC

This chapter presents the work that has been done within the scope of this present work to get the planned ignition systems and corresponding parts installed to the CVCC and is segregated by the two ignition systems.

4.1 Motortech- State of the Art Inductive Ignition System

The outcome of my project done prior to this current work initiated the process of purchasing a new conventional inductive ignition system. The budget was the main constrain for purchasing a new ignition system and the option of simultaneously igniting two spark plugs became the only demand for the new inductive ignition system. Recommendations from former PhD. Candidate Maximilian Malin and previous purchase from the institute from the German based company Motortech, led to month long e-mail correspondence with their Sales and Service Engineer, Rafael Canales. He provided us with the support we needed to finalize the order of a brand new ignition system, see final quotation attached in appendix A.2. The main parts that we order from Motortech can be seen in the schematics of the system in *Figure 33*, excluding the parts inside the red marked box, which involves the parts that monitor the position of the crankshaft and detonation in each cylinder.

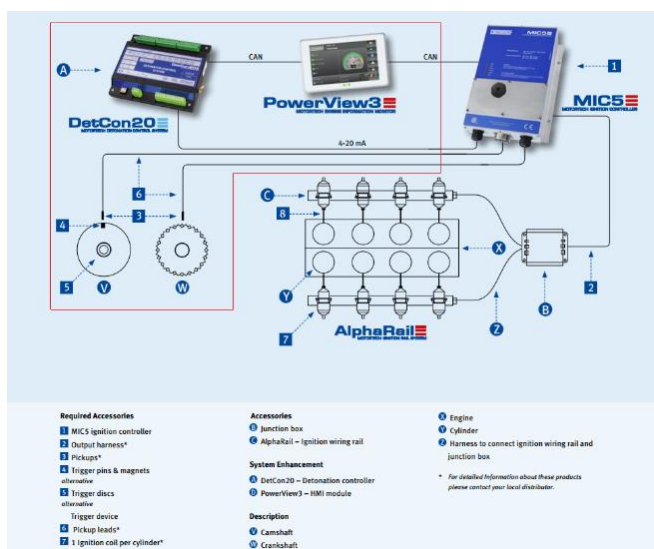


Figure 33: Schematics of The Conventional Ignition System from Motortech

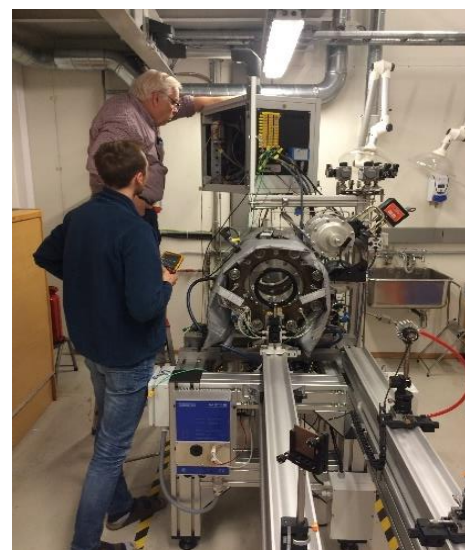


Figure 34: Installation and Implementation of the System

The MIC5 Controller is designed for gas engines up to 20 cylinders and is fully programmable, where the duration of the spark, the energy delivered (maximum 700 [mJ]) and ignition sequence can be adjusted to mention some adjustable parameters [39]. To accomplish a simultaneous ignition for this system, Senior Engineer Frode Gran installed a programmed Arduino Card, see *Figure 34*, which generates a fake pick up signal. This had to be done since the ignition controller uses the pick-up signal to determine the trigger time for each of the spark plugs in a normal engine. This signal, produced by the card, is used as a trigger signal for the two separate coils so that they initiate the spark at the same time.

The shielded high tension leads and coils were also an important factor for us since the electromagnetic noise produced in the conducting leads could influence other systems attached to the CVCC. This had been reported before when unshielded cables were used with the old ignition system.

Senior Engineer Frode Gran did the electrical wiring and programming of the ignition controller and connected the ignition controller to the Control PC, while PhD candidate Vladimir Krivopolianski and myself assisted in the assembly of the system to the rig, see *Figure 35*.



Figure 35: The Conventional Ignition System Installed on the CVCC

4.1.1 Design and Manufacturing of M18 Rig Plugs for the CVCC

The new ignition system from Motortech involved the use of two M18 spark plugs. This decision of using a M18 spark plug resulted in the need for a M18 compatible rig plugs for the CVCC. The previously used rig plug is compatible for M14 spark plugs only, and hence two M18 rig plugs for the CVCC had to be machined for this purpose.

Modifications and upgrades of the previous plug were discussed with PhD. Candidate Vladimir Krivopolianski. Firstly, the protrusion of the spark plug into the chamber had to be to such an extent that the spark was more than just aligned with the inner diameter of the CVCC. This would reduce the quenching effects and the barrier for a free propagating flame front. Then the curvature of the plugs facing inwards would be machined so it was aligned with the inner diameter of the CVCC. This would further increase the total volume of the rig compared to the previous rig plug with a plane cut. A 3D model was made in Catia, see appendix A.3 for the technical drawings, and then machined by Engineer Gunnar Bremset. The finished M18 compatible plug for the CVCC can be seen in *Figure 36*. The curvature for the rig plug has not been done at the present moment, but the plug for the pressure equipment has this curvature and is added for illustration only.



Figure 36: Final Outcome of Rig Plug for M18 Spark Plugs

4.1.2 Out leaning Program

In this chapter I will explain the out leaning process for the gas composition, and how we plan to implement this in our test procedure. This out leaning process was one of the objectives for this present work to evaluate the new ignition systems regarding their capability to ignite leaner mixtures.

4.1.2.1 Lowering the energy content

One very important parameter is the air/fuel ratio λ , which is used to describe the combustion characteristics, see *Eq. (4.1)* [7].

$$\lambda = \frac{\frac{\chi_{Air}}{\chi_{fuel}}}{\left(\frac{\chi_{Air}}{\chi_{fuel}}\right)_{Stoich}} \quad (4.1)$$

The definition of lambda classifies the combustion in three categories depending on the λ value. The stoichiometric gas composition has exactly the amount of oxygen to achieve complete combustion with no excess of oxygen after the combustion, hence giving a value relative to stoichiometric combustion, see *Table 4*.

Rich mixture	$\lambda < 1$
Stoichiometric mixture	$\lambda = 1$
Lean mixture	$\lambda > 1$

Table 4: Lambda Classification Regarding Air Fuel Mixtures

To investigate the ignition capabilities of our two ignition systems, we wanted to do experiments where the gas composition was gradually changed. The idea was to add N_2 into the GMB, which would change the composition in such a way that the volume fraction of CO and O_2 would be reduced. By doing this step gradually and with a shot for each new composition, a threshold for the minimum volume fraction of CO could be identified.

Since we are not changing the amount of O_2 or CO in the gas bottle, the lambda value is not possible to use to indicate the difference. Instead the volume fraction and energy content introduced into the CVCC will be used. By decreasing the amount of CO that we introduced into the chamber, the density of the injected gas for the pre-combustion can be increased which will allow us to simulate the environments described in chapter 2.5, without putting the CVCC at risk for the maximum pressure allowance.

4.1.2.2 Program for Initial Filling Process

A Matlab™ program was developed during this present work, see *appendix A.4*, which gives the corresponding volume fractions and partial pressures of CO, N₂ and O₂ to be filled in the GMB. The filling process is described in chapter 2.4. This program utilizes the ideal gas law *Eq. (4.2)* and calculates all the needed variables based on given parameters. These variables and parameters are further used as input for the out leaning program, see next chapter.

$$PV = mRT \quad (4.2)$$

The most important parameters and variables are presented in *Table 5*.

After Combustion			Before Combustion		
Vol % O2	21,00	[%]	Vol % O2	29,42	[%]
Vol % CO2	23,87	[%]	Vol % CO	21,32	[%]
Vol % N2	55,13	[%]	Vol % N2	49,25	[%]
Mass fraction O2	20,57	[%]	Mass fraction O2	32,26	[%]
Mass fraction CO	32,15	[%]	Mass fraction CO	20,46	[%]
Mass fraction N2	47,28	[%]	Mass fraction N2	47,28	[%]

Table 5: Gas Composition for Pre- Combustion

4.1.2.3 Program for Out Leaning Filling Process and Procedure

The outcome of this Matlab™ program was the volume fraction of CO after adding an amount of N₂ to the GMB after a number (n) of fillings of the CVCC, see *appendix A.5*. This would lower the energy content proportional to the mass of CO injected to the CVCC. The lower flammability limit for CO is indicated in the graph and shows the minimum volume fraction [%] of CO that has to be present for supporting a combustion in air in standard conditions [40]. This lower flammability limit will most likely be downshifted in a pressurized environment like the CVCC, but literature on this topic indicates a more complex relation, where many factors influence the limit [41].

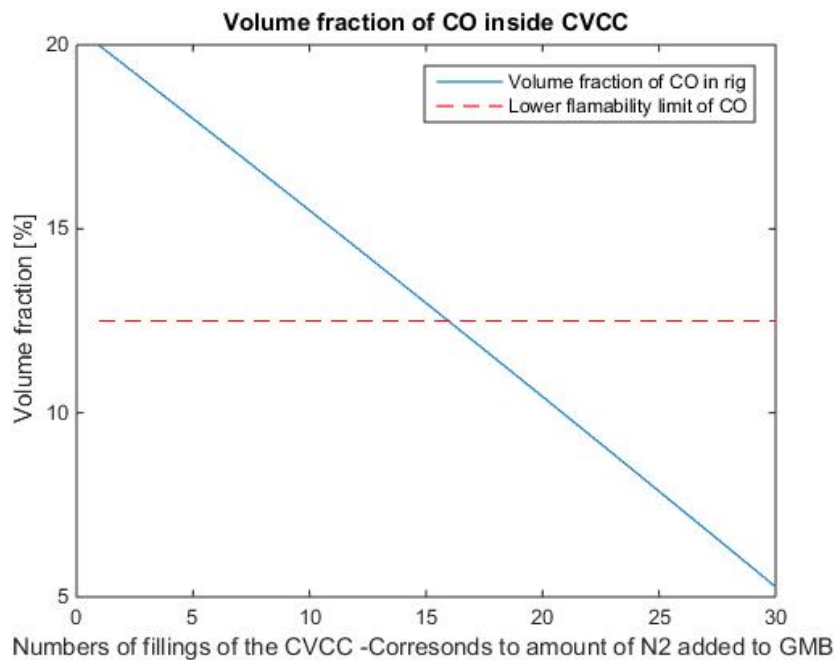


Figure 37: Volume Fraction of CO Depending on Added N₂ to the GMB

The filling process would initially be as described in *chapter 2.4*, but then after having carried out n fillings of premixed gas to the CVCC, with a filling pressure of 10 [bar], the GMB would be filled up to 40 [bar] again with N₂. After having added a specific amount of N₂ in the GMB, the mixing process, would have to be executed to ensure a well-mixed composition of the gas.

4.2 Corona Discharge Ignition System

Initiating the pre-combustion with Corona is regarded as the most promising ignition method to be used for pre-combustion for our CVCC. This is due to its physical nature as presented in chapter 3.2.3.4. The following chapter presents the theory, design and work done to install the Corona system to the CVCC. *Figure 38* shows an illustration of the system.

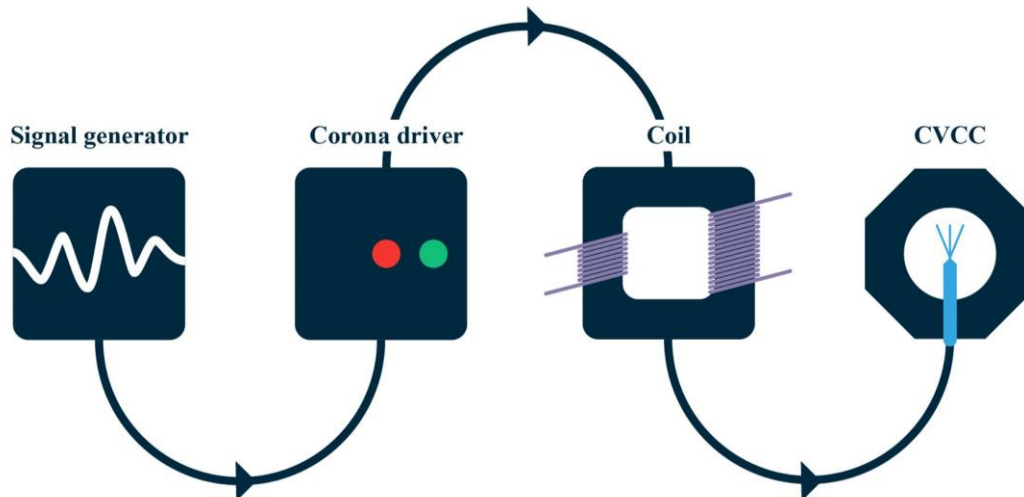


Figure 38: Illustration of Corona Discharge Ignition System

4.2.1 Corona Discharge Ignition Driver

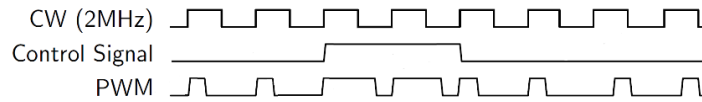
Øystein Smith and some fellow students from the Omega Workshop managed to design and assemble the TK500-Driver also called a DRSSTC-Double Resonant Solid State Tesla Coil. The preliminary user guide is attached in *Appendix A.1*, and a more comprehensive manual is announced to be finished during the spring of 2017 as a part of Øystein Smith's master thesis. *Figure 39* shows the interior of the driver and all the components installed inside the suitable black chassis box.



Figure 39: The Corona Driver

4.2.1.1 Controlling the Driver

As the illustration in *Figure 38* shows, the driver needs input in terms of a signal. This signal can be modified to adjust the streamer length and hence work as a voltage regulator for the driver, see *Figure 40*.



*Figure 40: Signal to the Driver for Output Control*¹²

The PWM is the acronym for Pulse Width Modulated and regulates the output from the driver by adjusting the pulse width; a shorter pulse width results in a shorter spark and vice versa, see *appendix A.1*. During the initial testing of the system, Øystein Smith will provide a duty machine which controls these parameters, but these signals can easily be generated and controlled from the Labview PC in the control room.

4.2.1.2 Tuning the Driver

The finished TK500-Driver from the Omega workshop needed to be synchronized to the capacitance of the rig. This had to be measured and calculated so that the resonant circuitry on the driver would fit the CVCC. The analogy of this could be seen as the driver's ability to produce the harmonic resonance frequency of the CVCC and more precisely, the secondary circuit, see *Figure 41*. Only by having this tuned will the resonance circuitry of the driver produce the voltage needed to generate corona streamers ideally.

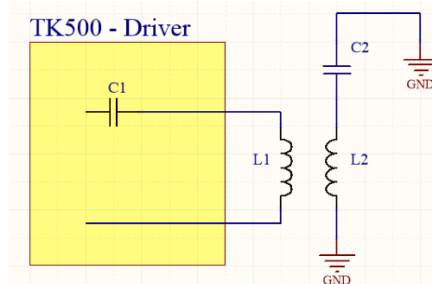


*Figure 41: Simple Circuit Presentation of the System*¹²

Øystein Smith conducted the test with the use of an oscilloscope and duty machine that produces the different frequencies, see *Figure 42* for the setup of the test.

¹² See Appendix A|.1

Three different load conditions were measured with the duty machine with different and known capacitors inside the driver. Calculations done by Øystein Smith, gave the resonance frequency of 320 [kHz] for the secondary circuit and modified spark plug, see *chapter 4.2.2*, inside the CVCC. This value gave the inductance for the primary coil at 14.6 [μ H].



Figure 42: Tuning the Driver

4.2.2 Corona Electrode- The Modified Spark Plug

In this chapter I will present the theory of conventional spark plug design and first design and prototype made for the corona ignition system.

4.2.2.1 Spark Plug Basics

The spark plug has over the year become more sophisticated and robust in terms of wear and tear, but the general components has not changed much since they first saw daylight in the latter half of the 18th century [42]. The spark plug is a component which main function is to provide an electrode gap where the high-voltage discharge occurs. Due to environment the spark plug is subjected to it has to withstand high pressures and high thermal shocks. The spark plug part, which protrudes from the cylinder head, is also subjected to chemical reactions where especially the ground electrode is affected to such a degree that the spark plug has to be maintained or changed from time to time.

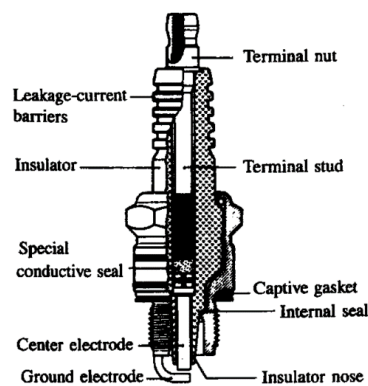


Figure 43: Cutaway in a Spark Plug [7]

Figure 43 shows the cutaway of conventional spark plug. This typical spark plug design consists of mainly three components: an insulator, electrodes and a shell [7]. For the insulating part of the electrode, Aluminum Oxide ceramics (Al_2O_3), commonly referred to as Alumina, is normally used. This material has several benefits that make it a good insulating material. The most important parameter is the dielectric strength. This property indicates the voltage level the material will withstand before it starts to conduct electricity. Alumina has the tensile and compression strength that is required in addition to the thermal shock resistance that the spark plug is constantly subjected to.

High temperature and corrosive gases inside of the camber put a lot of strain on the electrodes in terms of material, so high-nickel alloys are normally used for the electrodes. The terminal nut connects the spark plug to the ignition harness and conducts the high voltage through the terminal stud and to the center electrode. The special conductive seal is normally a glass or a spring with an internal resistance to minimize the electromagnetic noise. This also works as a mechanical anchoring between the terminal stud and the center electrode under fluctuating gas pressures.

The ground electrode is mounted on the lower part of the housing of the spark plug and conducts the high voltage to the grounded engine block. The housing and the conducting terminal nut, stud and center electrode are insulated from each other to prevent flash over.

4.2.2.2 Concept and Materials

The task was to introduce the high voltage generated by the Corona driver into the CVCC where the pressure and temperatures can reach 100 [bar] and 1800 [K] respectively. This puts a lot of strain on the electrode and especially the sealing between the housing and the conducting electrode. To minimize the cost and production time we decided to use a M18 sparkplug and modify it for our purpose.

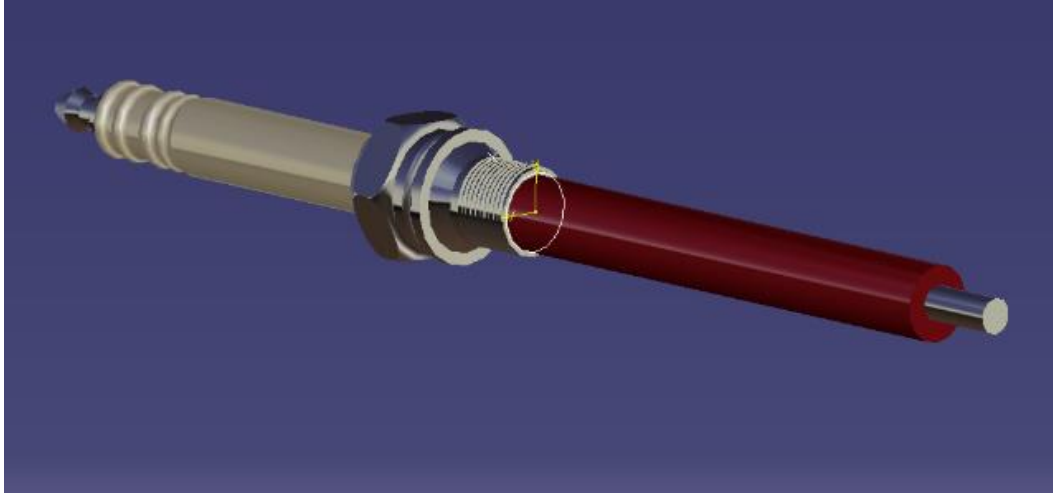


Figure 44: 3D Model of Spark Plug Made in Catia

Figure 44 shows the initial design as a model made in Catia. The idea involved minor modification, where the central electrode is extended and a tube of alumina is used as insulation, seen as red in Figure 44. The alumina tube was provided by the senior Researcher Ove Paulsen working at SINTEF for the department of materials and chemicals at Gløshaugen. The Alumina tube has an outer diameter of 10 [mm] and an inner diameter of 6 [mm] giving a thickness of 4 [mm]. The dielectric strength of that particular tube is 32 [kV/mm] giving a total of 128 [kV].

To seal the air gap between the alumina tube and the insulator nose on the spark plug, we planned to use ceramic glue purchased from senior engineer Astrid Salvesen at the Glass Blowing Workshop at NTNU, Gløshaugen. This part was believed to be the weak link on the modified spark plug since this would be the shortest path from the conducting electrode to ground. The estimated voltage level from the corona driver was at current time believed to be below 50 [kV] and hence setting some minimum isolating properties on the glue to prevent unwanted flash over.

The alumina tube, see *appendix A.6*, would be drilled in one of the ends to get the same conical shape so that the insulator nose and tube would have a corresponding geometry. The length from the center electrode and the spark plug housing was measured to be approximately 12 [mm]. The dielectric strength of the ceramic glue named [989FS](#) from Cotronics has a stated dielectric strength of 200 [volts/mil], which corresponds to 8 [kV/mm]. This makes the total dielectric strength of the crevice between the alumina tube and spark plug insulation nose 96 [kV] if the glue is applied correctly with no trapped air inside. If air is present in the glue the dielectric strength will be drastically decreased since the insulating properties of air is much less than alumina [43]

Mechanical work on the modified spark plug was planned with staff engineer Kristian Minde and Engineer Gunnar Bremset at the mechanical workshop at the department of Marine Technology at Tyholt. A pointy tip at the center electrode was also implemented in the plan to create a strong electrical field gradient.

4.2.2.3 First Prototype of the Modified Spark Plug

The modification of the spark plug was executed according to the plan and the materials were gathered and purchased as explained in the previous chapter. The modified spark plug can be seen in *Figure 45* with additional insulating tape over the crevice between the spark plug housing and the ceramic tube.



Figure 45: First Modified Spark Plug

The first test with the alternative corona ignition system will be the ultimate test if the spark plug will withstand the voltage generated by the corona driver and will therefor generate corona at the tip of the extended electrode. *Figure 46* shows the location of the extended spark plug tip inside of the CVCC.



Figure 46: Position of Modified Spark Plug Tip inside the CVCC

4.2.3 Coil

This chapter briefly presents the basic principles and physical laws for the coil and how it was made by the workshop Omega at NTNU

4.2.3.1 Coil theory

A current that flows through a wire will create a magnetic field around the conducting wire [44, 45]. By arranging the wire in a helix shape the electromagnetic field will be added in the center of the coil, see *Figure 47*.

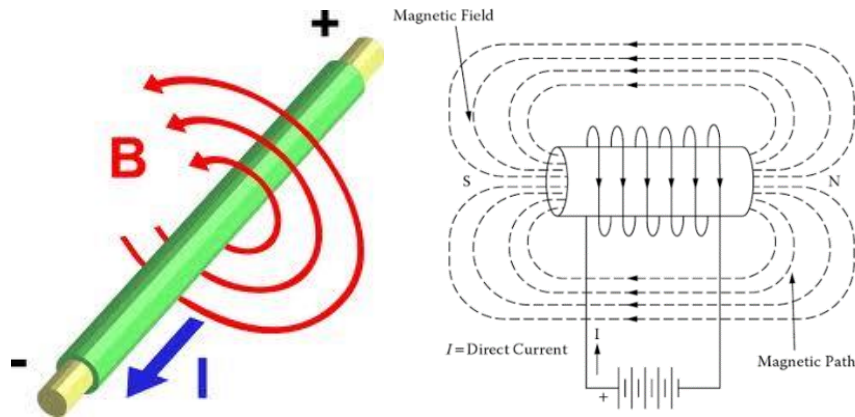


Figure 47: Electrical Field Lines Around Conducting Wire¹³ and Coil

Faradays law *Eq.(4.3)* shows the relationship between induced voltage in a coil by a changing magnetic field where N is the number of windings of the wire in the coil, B is the magnetic flux which penetrates the perpendicular area A and is known as coil area (surface area) when looking lengthwise through the coil [46].

$$V_{induced} = -NA \frac{dB}{dt} \quad (4.3)$$

Transformers use these relations and can step a voltage up and down by adjusting the numbers of windings, see *Figure 48*.

¹³ <http://onetesla.com/tutorials/how-a-tesla-coil-works>

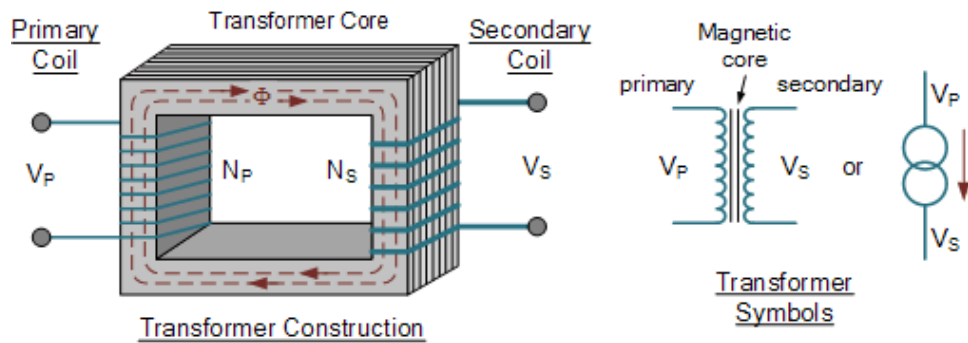


Figure 48: Illustration of Transformer Basic Construction ¹⁴

This figure illustrates a transformer where the primary circuit with N_p windings around the iron core and with a V_p voltage applied. If a current is present in the primary circuit, this will create a magnetic field seen as field lines around the iron core, which again will induce a voltage V_s in the secondary circuit depending on the number of windings N_s . This relationship is presented in Eq.(4.4)

$$\frac{N_1}{V_1} = \frac{N_2}{V_2} \quad (4.4)$$

As Eq.(4.4) shows the theoretical voltage induced in the secondary circuit is proportional to the number of windings in that coil, but there are several factors which influence the rate of transformation. The distance between the primary and secondary coil will determine the amount of the electromagnetic field that will interfere with the secondary coil

4.2.3.2 Making the Coil

Øystein Smith and his fellow students made a rig where they were able to rotate the tube where they applied the wire, see Figure 49

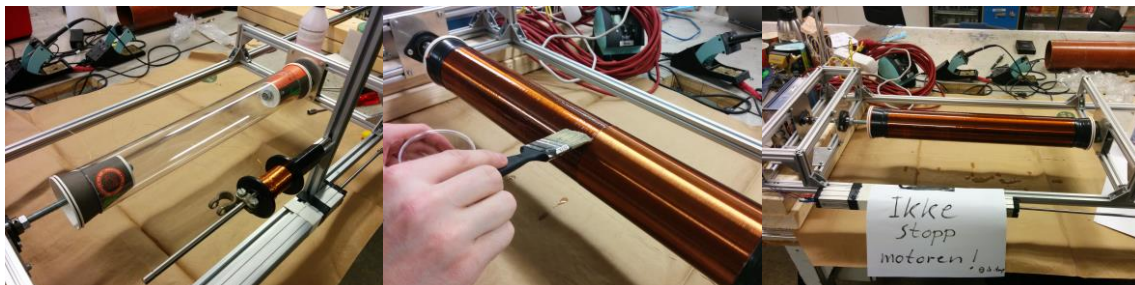


Figure 49: Omega Workshop Making the Coil

¹⁴ <http://www.electronics-tutorials.ws/transformer/transformer-basics.html>

4.2.4 Faraday Cage for the Coil

This chapter explains briefly the concept of electromagnetic shielding with the use of faraday cage and the design and outcome made for this purpose.

4.2.4.1 Theory of Electromagnetic Field and Faraday shielding

The coil that was made by the workshop at omega, see *Figure 50*, increases the voltage output from the driver. When current is flowing through the coil a magnetic field is set up. This magnetic field has energy in terms of electromagnetic waves that can interfere with other systems connected to the CVCC [47], and to prevent this phenomenon a faraday cage is necessary.



Figure 50: The Coil Made by Øystein Smith and Fellow Students at the Omega Workshop

The principle of a faraday cage is well known and will only be presented briefly [48, 49]. The faraday cage can have many shapes and be made out of many different materials depending on what kind of electromagnetic waves you want to shield, but the walls must have a conductive layer [50]. When the electromagnetic field is present, free charge on the enclosure will then relocate itself so that they oppose the electromagnetic field, induced by the coil itself, and exactly cancel out the electromagnet field, see *Figure 51*.

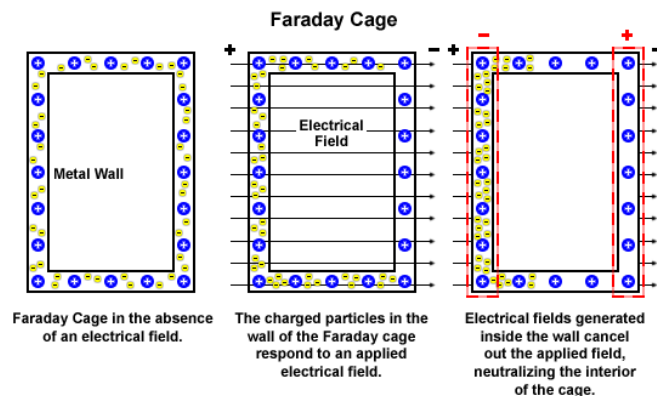


Figure 51: Electrical Field and Faraday Cage¹⁵

¹⁵ <https://nationalmaglab.org/about/around-the-lab/what-the/faraday-cage>

4.2.4.2 Design and final outcome

The specification for the shielding faraday cage had few constraints. The cage needed dimensions so that the coil could easily be mounted on the inside, robust and made with a conducting material such as steel. A 3D model was made in Catia, see *Figure 52* and *Appendix A.7* for technical drawings.

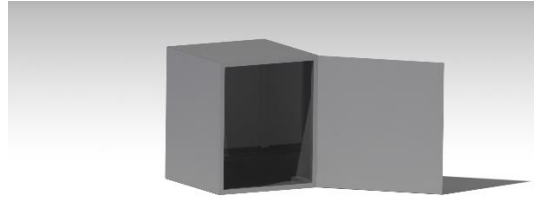


Figure 52: 3D Model of Faraday Cage Made in Catia

Staff Engineer Oddvar Paulsen gave the task to a young apprentice at the workshop at the department of marine technology and the final outcome of the faraday cage can be seen in *Figure 53* with the coil mounted on the inside with four bolts and nuts in each corner, which simplifies movement of the equipment. The hinged front panel was also modified to a detachable panel with corresponding holes in the front with M10 threaded holes.



Figure 53: The Coil Installed inside the Finished Faraday Cage

4.2.5 Final Set-up for the Corona Discharge Ignition System

Before the first initial test with all the above mentioned equipment, the system was installed to the CVCC. The ignition system is, according to Øystein Smith, capable of generating a theoretical maximum of 33 [cm] corona streamers, which is equivalent to a voltage output of 1 [MV], when the dielectric strength of air is 3 [MV/m] is assumed [26]. This voltage output can be adjusted by turning a knob on the duty machine, so that we can produce the wanted streamer length that is less than the distance from the tip of the electrode and to the closest surrounding grounded object, e.g. the inner face of the CVCC to prevent flash over.

Chapter 5

Experiments and Results of the Ignition Systems

This chapter will present the test that we conducted for each ignition system and corresponding results and actions that we needed to initiate after having analyzed the results for the alternative ignition system.

5.1 Motortech Ignition System

The system had been installed, implemented into the Labview PC in the control room and function tested by Senior Engineer Frode Gran in atmospheric conditions, where the spark was inspected visually, before we started the initial test. PhD Candidate Vladimir Krivopolianskii wanted to conduct both test of the ignition system and lean out the gas mixture. The reason for this was that the amount of available gas (N_2 , CO and O_2) was limited. Several aspects of the experiment were discussed like the position of the spark plugs, and how we could conduct the out leaning process according to the process described in *chapter 4.1.2.3*.

5.1.1 Test procedure

A Measuring Protocol (MP) was made in cooperation with PhD Candidate Vladimir Krivopolianskii, see appendix A.8. This MP ensures that the experiment is conducted as planned and contains all the boundary conditions given for the test.

The number of possible fillings of the CVCC and available time before the mixed gas is regarded as old set some constrains for our experiment, as explained in *chapter 2.4*. To establish a basis for comparison between the old ignition system and this ignition system, we had to have similar conditions to those David Koch had when he conducted his experiment MP99. The reason for only having that scarce amount of comparable data is due to newly installed heating element inside the CVCC which reduced the total volume [3]

The two first points on the MP104 would be executed with first one spark present and then two sparks present respectively and with the same gas composition as *Table 3* in *chapter 2.4* shows, see spark plug location numbering in *Figure 54*. Then the proceeding points regarding the MP would be to a gradual out leaning series, where a specific amount of N_2 was added to the GMB. PhD candidate Vladimir Krivopolianskii also wisely suggested an improved out leaning process where a specific amount of N_2 was added to reach a corresponding volume fraction of N_2 instead of always filling the GMB up to 40 [bar] since that could potentially result in a very large difference in the volume fraction. By narrowing the difference between each volume fraction from one test to another, the initial lean limit could be indicated in a much more specific interval. To confirm such limits a number of equal experiments have to be conducted to have sufficient data to predict the limit based on a statistical methodology. This MP104 had as its main objective to test the ignition system in a pressurized environment and perform the out leaning process. *Table 6* shows the boundary conditions for the MP104 experiment for the high-speed camera and the test environment.

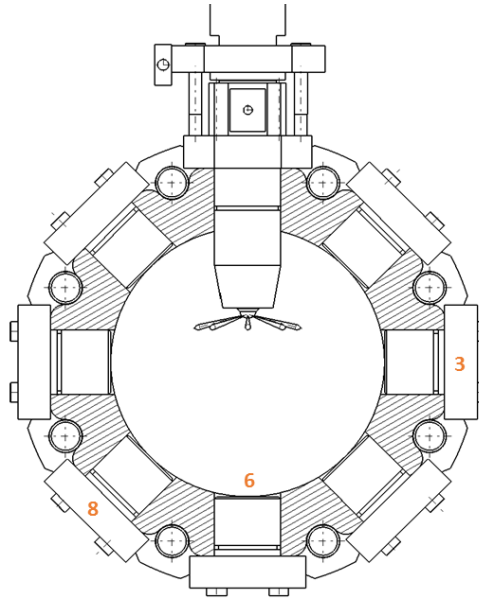


Figure 54: Illustration of CVCC and Spark Plug Positions

Settings	Value	Unit
Pressure in CVCC before pre-combustion	8 ± 0.1	[Bar]
Frame rate	500	[p/s]
Resolution	640x544	[-]
Aperture	f/5,6	[-]
Shutter time for direct imaging	1/25000	[1/pic]

Table 6: Important Parameters and Boundary Conditions for the Test

5.1.2 Results of MP104

The MP104 was executed over two days with PhD Candidate Vladimir Krivopolianski. Due to several reasons, the MP104 was not conducted according to its initial plan, see *Appendix A.7*. The points we conducted are presented in *Table 7*. The pressure data and corresponding photographic material from each of the points was recorded and is separated by the following chapters according to purpose of the conducted test.

Point	Volume Fraction of CO [%]	Spark plug position
1	20,04	8
2	20,04	3/8
3	19,21	3/8
4	19,21	6
5	17,74	3/8
6	15,85	3/8
7	15,85	3/8
8	15,85	3/8

Table 7: Conducted Points under MP104 regarding Vol [%] of CO and Spark Plug Position

5.1.2.1 One Vs. Two and Functionality Testing

Figure 55 and the image on the left side shows the flame front propagating from the spark plug at position 3 while the image on the right side shows point two of MP104 with the first successful twin spark ignited pre-combustion fired in the CVCC.

Both pictures are taken at the same time after ignition (904 [ms]).

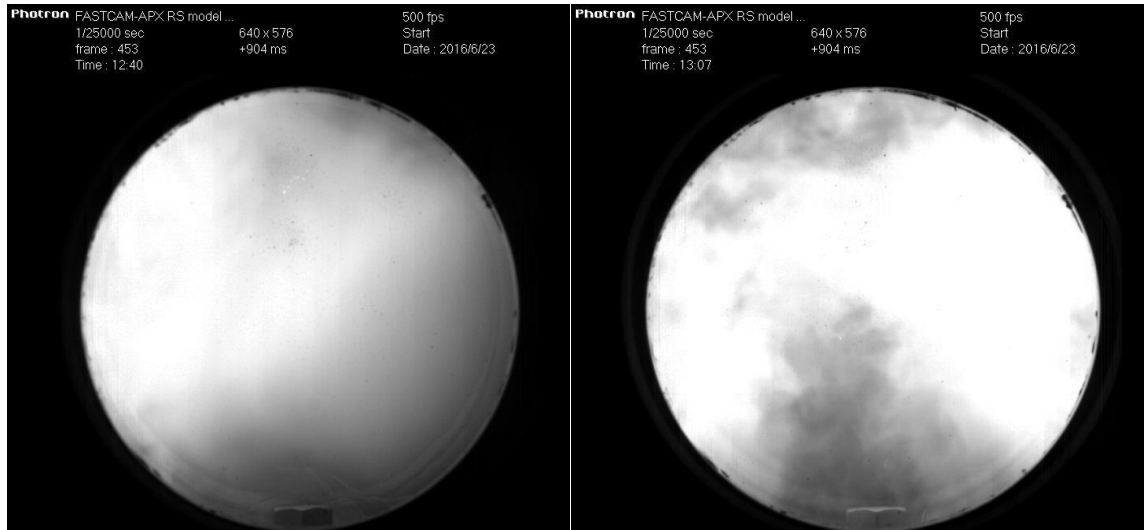


Figure 55: Images of Flame Front Propagating from Spark Plug Position 3 and 3/8

The pressure data recorded from each test is presented together in the graphs in Figure 56. As literature indicates [51, 52], a higher energy content delivered to the ignition phase increases the flame growth, pressure and combustion efficiency to mention some important combustion parameters for the ignition. This is seen in Figure 56 where point two shows both a high pressure recorded and at a slightly earlier time instance.

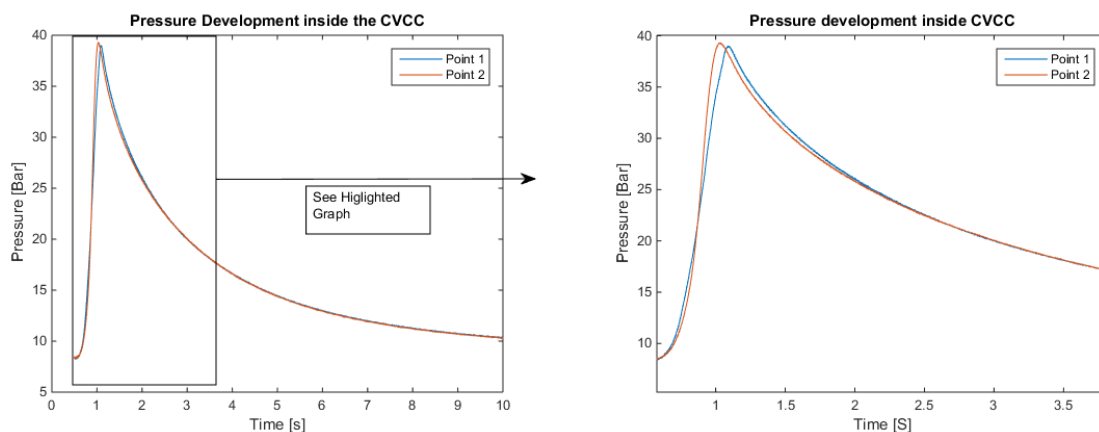


Figure 56: Pressure Development Inside CVCC for Point 1 and 2 for MP104

5.1.2.2 Adding N₂ to the GMB

After having conducted two successful tests, we proceeded with adding a small amount of N₂ to the GMB and initiated the mixing process before conducting the same test procedure as with point 1 and 2. *Figure 57* shows point 3 and 4 respectively with same gas composition. We recorded only successful ignition at position 6 for point 4.

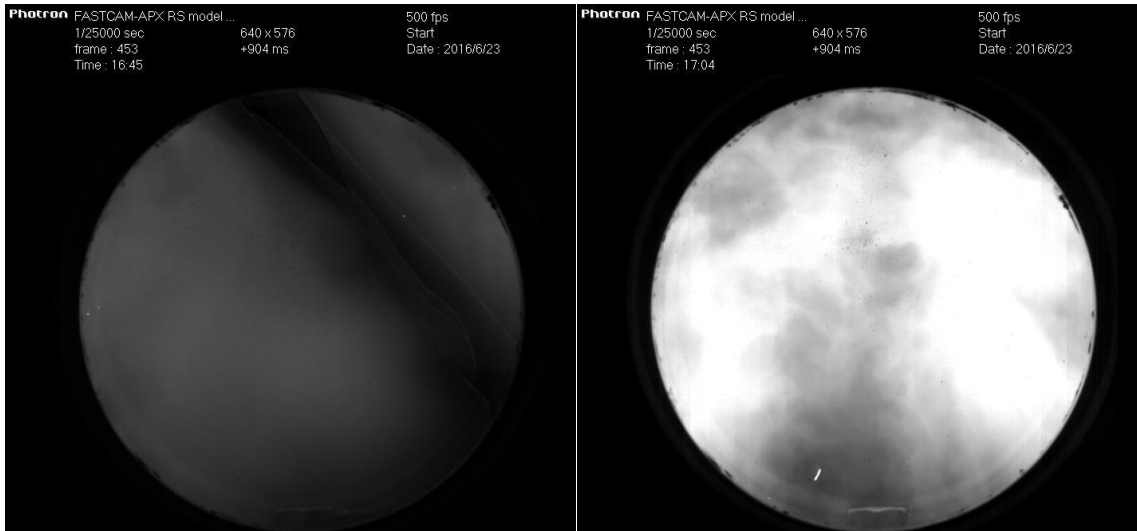


Figure 57: Images of Flame Front Propagating from Spark Plug Position 3/8 and 6

The pressure data from these two points are combined to highlight the difference between single and twin spark plug initiation for the pre-combustion and the use of spark plug position number 6, see *Figure 58*. This result contradicts the literature and what we could expect from point 1 and 2 since the highest pressure and most rapid combustion initiation is recorded for point 4. This might be explained with a more suitable spark plug position where the flame growth is less effected by the inner heating element, as mentioned as a plausible effect of this added equipment [3]. It could also be a combined effect of a slightly higher filling pressure of the CVCC, which is recorded to 0.1 [bar] in favor for point 4, but this difference could be as much as 0.3 [bar] due to given margin of error in pressure sensor and hence explaining the higher peak pressure for this particular test.

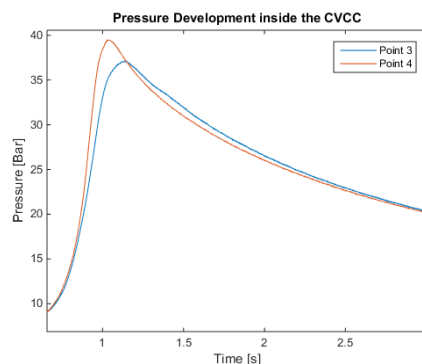


Figure 58: Pressure Development Inside CVCC for Point 3 and 4 MP104

The remaining points are presented in the figures where the three last points on the MP104 are given as average for those recorded data since they represent the same test conditions, seen as Point 6/7/8 in *Figure 59*. The previous points with equal spark plug position and thus the same test conditions, besides the gradually changed gas composition, are presented in the same graph to illustrate the tendency of less injected fuel in the CVCC.

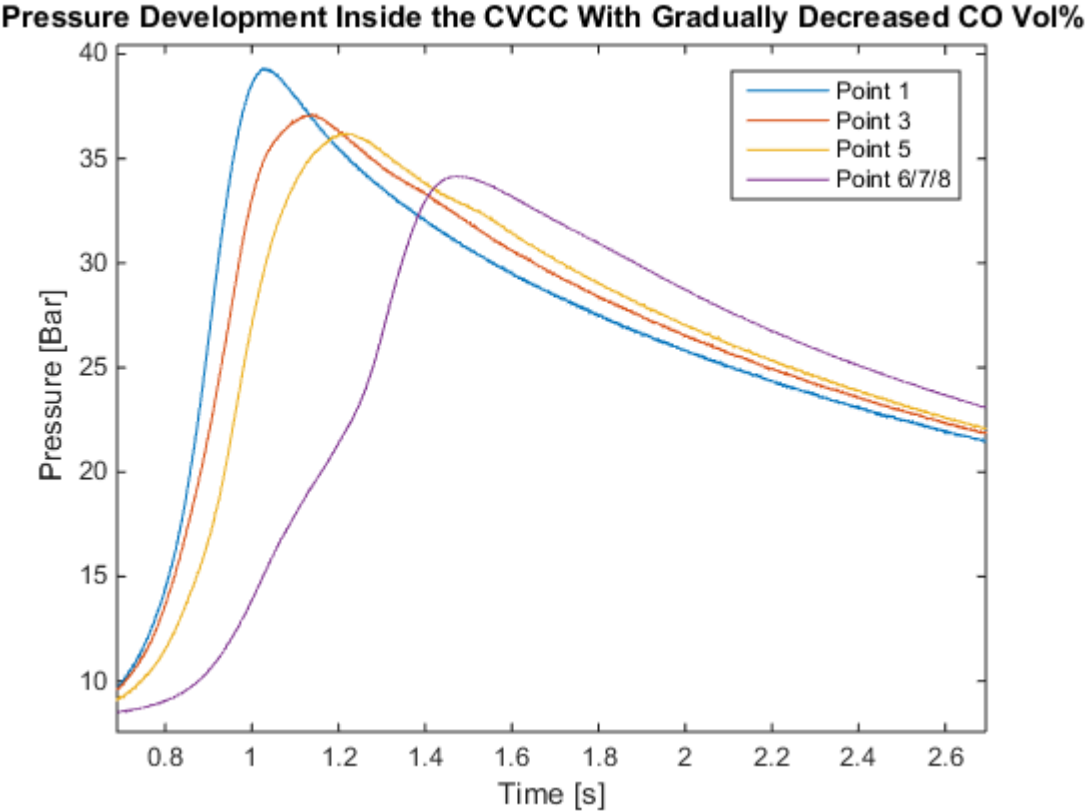


Figure 59: Pressure Development Inside CVCC with Gradually Reduced CO Vol [%]

5.1.2.3 “New” Volume Fraction of CO in CVCC During MP104

After we had conducted point 8 on our MP104, we proceeded by adding one last amount of N₂ according to specific out leaning program developed, giving a volume fraction of 14 [%], see *Appendix A.7*. We were not able to ignite this gas composition, as we expected, when we regard how close we are to the lower flammability limit of CO, at 12,5 [%] at atmospheric conditions. After analyzing the filling process for the out leaning procedure, after we had finished the MP104 indicated that the volume fraction of CO that had been calculated prior to the experiment was not accurate.

Figure 60 shows the procedure and corresponding values for pressure of GMB, partial pressures for each species, and most importantly the volume fraction, see *Appendix A.9* for calculation.

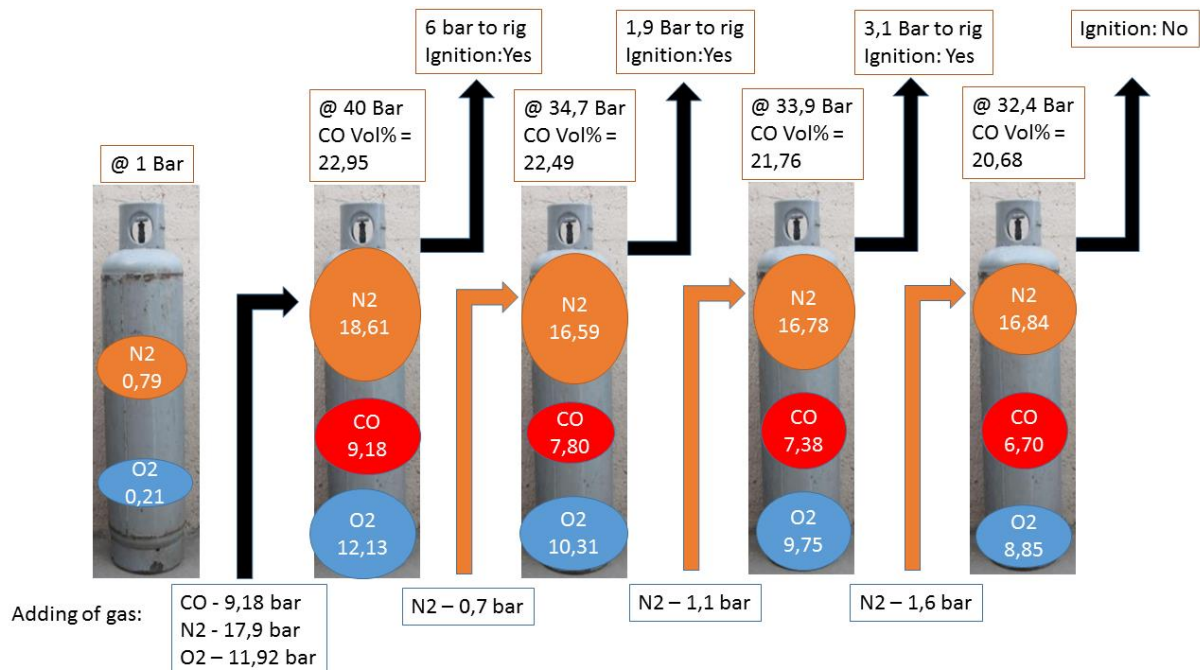


Figure 60: Out Leaning Process and Gas Composition

5.1.3.4 Result of MP99

David Koch conducted similar tests, while he did his master thesis, where heating elements and insulating material was installed to the CVCC to improve the inhomogeneous temperature field [3], see *Appendix A.9* for MP99. The three first points were executed without the use of the fan, or no other electrical heating, resulting in the same boundary conditions as for MP104. This test was initiated with the old ignition system, as briefly explained in *chapter 2.6*. The pressure data from this test is presented in the first graph in *Figure 61*.

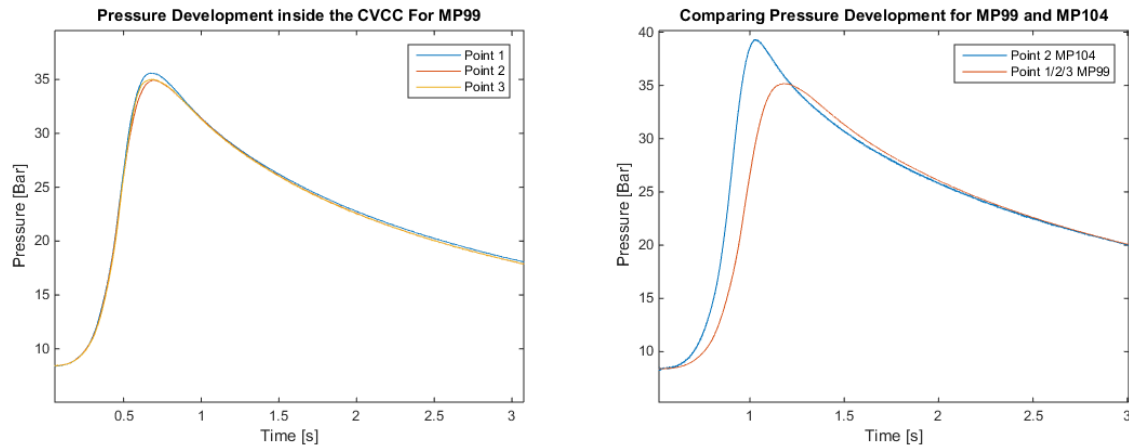


Figure 61: Pressure Development Under Similar Conditions for MP99 Versus MP104

Second graph shows the result from MP99 where all those three points are averaged and compared with the MP104 and point 2 where both spark plugs initiated the pre-combustion. There is approximately a 4 [bar] difference in the pressure peaks between those two ignition methods. These findings fit existing literature and what should be expected when a more powerful ignition system supplies substantially more energy into the ignition phase.

5.2 Corona Discharge Ignition System

The test for the alternative ignition system was conducted during the summer with Øystein Smith and PhD Candidate Vladimir Krivopolianskii- when he had the opportunity to attend. The objective of these tests was to conduct safe and controlled testing of the whole system. The safety was a main concern due to very high voltage levels [53]. The results of each test and new actions after the conducted test are presented in different chapters depending on spark plug design.

5.2.1 Test procedure

The system was connected and rigged according to *Figure 38*. Then the designated operator for the driver would turn on the driver as described in *Appendix A.1*. If one of the safety buttons is pressed under operation, seen as red buttons in *Figure 62*, the driver will cut the power for safety precautions. The duty machine was operated by Øystein Smith and had to be tuned to find the correct voltage level. All other systems connected to the CVCC were turned off and detached if possible in case of high voltage flowing through this expensive equipment.



Figure 62: Front Panel and Safety Buttons on the Driver

5.2.2 Result Test I- Modified Spark Plug I

The first noticeable action was a small noise after the duty machine was slowly adjusted from its initial position, where the signal to the driver is flat. Then suddenly the noise became loud after the duty machine increased its driver signal, and the operator intentionally stopped the diver by pushing the big red button. We had visual contact with protruding electrode inside the CVCC, but did not see any flashover nor light glimpse. We inspected the spark plug and saw that the electrically insulating tape that we had applied had melted, see *Figure 63*. This ended the first test and implied that the weak spot in the spark plug had failed to withstand the voltage level and the ceramic glue had conducted the electricity through the crevice towards ground.



Figure 63: Detailed Picture of Scorched Insulating Tape After Test 1

5.2.3 Result Test II- Modified Spark Plug II

5.2.3.1 Modification

The first test indicated that the system worked as expected, but that the weak link in the modified spark plug made the wanted outcome impossible. We also discovered that the extended central electrode was loose, but not where our extension had been crimped, but rather inside the internal sealing. To verify whether this spark plug was still usable we connected the terminal stud and the center electrode to a multimeter to measure the resistance. The result was at that current time a new discovery and measured 50 [k Ω]. We measured several spark plugs and they all had the same internal resistance independent of the manufacturer. This internal resistance is used to reduce the radiated ElectroMagnetic Interference (EMI) [54], which in our case could result in higher produced voltage from the driver.

We decided to make a new spark plug with no internal resistance and we tried to increase the insulating capability in that particular spot where the insulation failed on the previous spark plug design. The changes we decided to implement were based on the conclusions we reached after the first test. Removal of the internal sealing had to be executed by senior engineer Astrid Salvesen at the Glass Blowing Workshop at NTNU Gløshaugen, since they have the equipment to do such work with a material as delicate and hard as ceramics. Our initial attempt failed when using our in-house tools and equipment, see *Figure 64* [55].



Figure 64: Removing Internal Resistance Inside the Spark Plug

The internal spring with the resistance was removed and a steel piece was machined to fit on the inside to connect the terminal nut to the center electrode. To increase the insulating properties of the material, we decided to apply epoxy from Loctite® with a given dielectric strength of 23,3 [KV/mm] [56]. This is almost 3 times the threshold for the ceramic glue used on the first spark plug. The distance from the center electrode to the spark plug housing is measured to be approximately the same giving a maximum dielectric strength of 280 [kV]. This epoxy based insulation cannot be used in a hot environment, so this is only for experimental use in this phase of testing of this alternative ignition system.

5.2.3.2 Test and Result

Our second attempt to generate corona with the alternative ignition system was conducted as the previous test. The outcome of the second experiment was equal: we heard a very loud crackling noise and could see a clear and bright light emitted from the inside of the CVCC where the high voltage exceeded the dielectric strength of the applied epoxy and towards the nearest grounded piece which in this case was through the spark plug housing and the M18 plug.

5.2.4 Result Test III- Insulated Steel Rod

5.2.4.1 Modification

After two experiments where the insulation had been too weak in its capability to not conduct electricity, we decided to make very simple electrode with no crevice. We knew that the voltage generated by the driver could exceed several hundreds of kilo volts. We also decided to make the tip of the electrode very pointy to make sure that the electrical field on the tip would be as high as possible. Producing corona is highly dependent of the field and makes this process time consuming due do to methods involving laboratory work with trial and error.

This electrode would consist of a long rod machined out of steel with a pointy tip at one end and a shape so the spark plug connector on the high tension lead would fit. Same alumina tube would be used as for the previous test. *Figure 65* shows the electrode after staff engineer Kristian Minde had machined the electrode.



Figure 65: The 40 [cm] Machined Steel Rod with Pointy Tip and Terminal End Connector

5.2.4.2 Test and Result

The final test was conducted with the electrode protruding the CVCC and hold in place in the plug with a ring of rubber, see *Figure 66*.

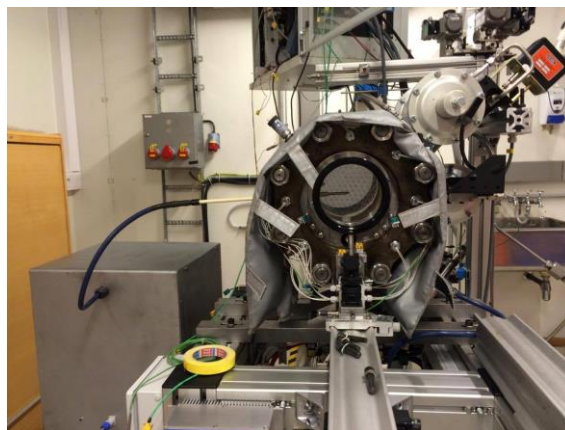


Figure 66: Test III Setup with the Electrode Protruding the CVCC

The result was not as expected as Figure 67 illustrates. What we see is arcs on the outside of the alumina tube propagating from the inner end and to the nearest ground, which in this case is the plug on the CVCC.

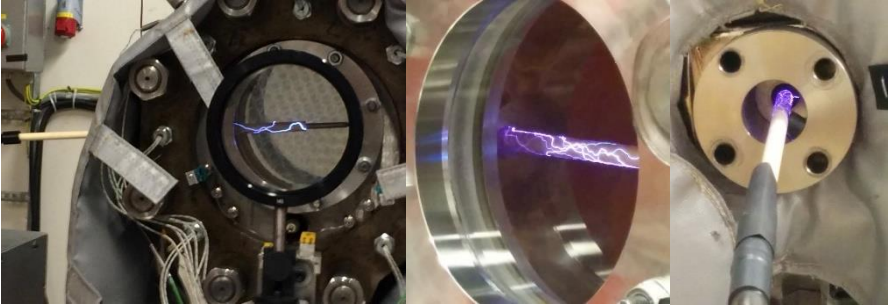


Figure 67: Visual Documenting Results from Test III

This flashover arcing result happens very abruptly when adjusting the duty machine and hence the voltage output could have a low sensitivity response. This should be the reason why we are not capable of tuning the duty machine to a lower level where the generated voltage should be at such a magnitude where some small corona streamers should be generated. We would expect that there was a transition phase where the electrical field would be sufficient enough to produce small corona streamers near the tip, as illustrated in Figure 68. But the voltage generates an electrical field around the electrode lengthwise resulting in a conducting surface.

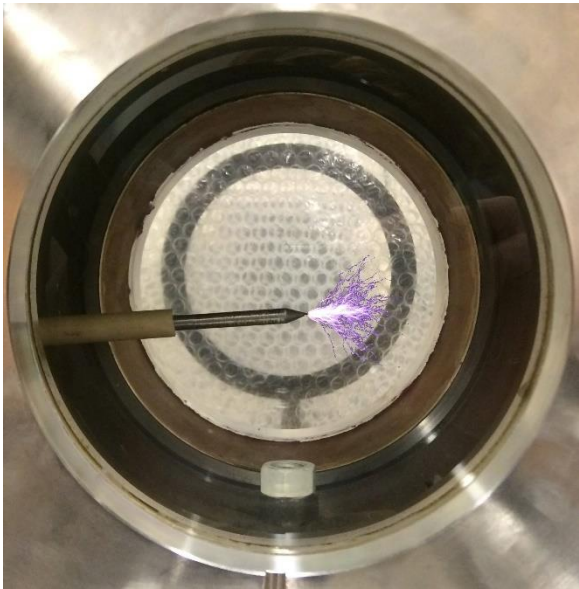


Figure 68: Illustrated Corona Discharge from the Tip of the Electrode

This final result of the alternative ignition system again showed that the high voltage produced by the driver is too high and no corona is present due to flashover between the electrode and ground.

Chapter 6

Conclusion

This chapter will present the conclusions on the ignition systems and an attempt to answer the postulated hypothesis will be made based on the results and observations from the conducted experiments during this present work besides the and my suggestions for further work.

6.1 Conclusion

The figure 2 and 3 in chapter 1.1 laid the basis for the postulated hypothesis for this master thesis where a more symmetrical ignition for the pre-combustion is believed to significantly improve the temperature field regarding the homogeneity inside the CVCC. This would be tested by two separate ignition methods that we purchased and assembled for this present work and by conducting experiments to collect data for analysis. The conventional ignition system from Motortech did not have the overhanging possibility of malfunctioning like the alternative ignition system did considering that the main parts of the corona discharge ignition system was made by fellow students and with in-house equipment. The installation of this conventional system is nevertheless a mayor improvement that increases the opportunities regarding spark plug setup and parameters such as ignition duration and energy output which substantially improves the capability of igniting leaner mixtures.

6.1.1 Motortech Ignition System

The experiment that we conducted for the conventional ignition system did indicate a faster pressure increase and hence better combustion efficiency when comparing single and double spark plug setup. To conclude based on only two experiments is not possible, but the results from the experiment indicated what is stated in the literature and our assumptions. The ignition system did ignite leaner fuel compositions due to additional amounts of N_2 in the gas mixture. What gas composition the ignition system is capable of igniting has to be investigated further. This will indicate what density level we can introduce into the CVCC without overshooting the maximum allowed pressure limit for the rig under pre-combustion.

The recorded data from our experiment does not provide the basis we need to draw any conclusions on whether the temperature field has been improved.

6.1.2 Corona Discharge Ignition System

None of the three spark plug designs of the conducted tests made us capable of producing corona inside the CVCC. Insulation is an important aspect of high voltage applications such as this one and has to be improved, so that the introduction of the high voltage into the CVCC is possible without producing the unwanted spark discharge between the electrode and the nearest earth connected part on the CVCC. The sudden arc discharge that we produced in all three tests made us question the sensitivity of the duty machine and its ability to gradually increase the signal in that critical area where the system could produce corona.

6.2 Suggestions for Further work

The work that is suggested to further investigate the temperature field is divided into two parts based on ignition method.

6.2.1 Motortech Ignition System

This is the only operational ignition system as of today and should be investigated further more for its ability to ignite leaner mixtures. That is the main objective for this ignition system: to be able to improve the simulated environment inside the CVCC. Here a similar procedure as conducted for the MP104 should be executed but with a more precise way of measuring the added components. The laboratory is currently improving the gas mixing arrangement where the ultimate goal should be the possibility to inject exactly the partial pressure of each component individually into the CVCC. This would reduce the time that is needed for a mixing arrangement and the unfavorable venting of deteriorated gas mixtures.

To investigate if the temperature field had improved with the dual spark ignited pre-combustion, we should have executed a similar experiment to document the unsymmetrical reactive shot. That would give a clear indication of whether the improvement of the dual spark ignition method would influence and result in a more symmetrical combustion. To investigate this issue, the fuel injector has to be positioned on the side of the rig so that the high speed camera can capture the sprays within the CVCC by using the direct imaging technique.

Another possibility for investigating if the temperature field has improved is by conducting tests similar to those of David Koch which he conducted for his master thesis [3]. He used a set of thermocouples placed in an organized structure on one side of the CVCC to get a picture of the temperature field inside the rig. This method is more expensive due to high cost for the thermocouples, but it provides a much more accurate picture than is possible with other methods.

6.2.2 Corona Discharge Ignition System

Focus should be to provide a signal to the driver that is more controllable in terms of sensitivity. That should at least make the output from the driver more controllable. But this does not address the voltage issue, which has proven to be a major problem when it comes to insulating the electrode. The alumina tube that we used does not have sufficient thickness to provide the insulation we need. If this parameter is increased, the threshold that the alumina tube can withstand will increase proportionally. An illustration of a possible design can be seen in *Figure 69* where it is illustrated along with the last spark plug design. Here the electrode with the insulating tube is integrated into the plug. By doing it this way the sealing issue is also addressed. This aspect was ignored in the last spark plug design we made due to time constrains in this present work. If ceramic glue is added both between the tube and the plug and the tube and the electrode then the part should be sufficiently sealed, which will prevent it from leaking when the CVCC is pressurized. This will be an important factor so that this ignition system could be used to initiate the pre-combustion. Depending on how the plug is designed, the shortest path from the electrode and to the grounded CVCC plug could be substantially increased, and thus providing insulation that can withstand voltage levels exceeding 0.5 [MV].

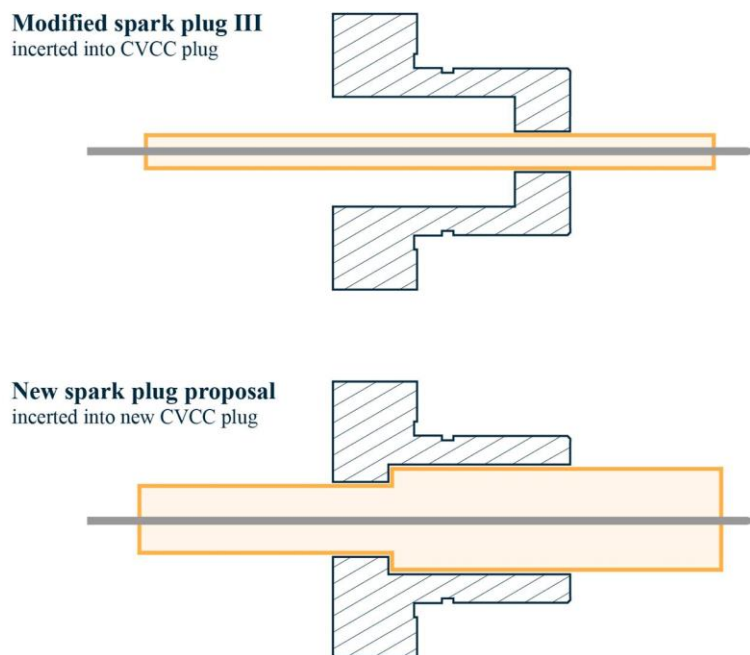


Figure 69: Illustration of Integrated Electrode in Rig Plug for Maximized Insulation

References

1. Meijer, M., et al., *Engine Combustion Network (ECN): Characterization and comparison of boundary conditions for different combustion vessels*. Atomization and Sprays, 2012. **22**(9): p. 777-806.
2. Baert, R.S.G., et al., *Design and Operation of a High Pressure, High Temperature Cell for HD Diesel Spray Diagnostics: Guidelines and Results*. 2009, SAE International.
3. Koch, D., *Improvement of a high-pressure high temperature combustion rig concerning the inhomogenous temperature field after pre-combustion*, in *ITV-Institut Für Technische Verbrennung 2015*, Aachen University.
4. Rygh, B.M., *An Experimental Study n the Application of Fish Oil as Fuel*, in *Department of Marine Technology*. 2015, Norwegian University of Science and Technology. p. 83.
5. Settles, G.S., *Schlieren and Shadowgraph Techniques: Visualizing Phenomena in Transparent Media*. 2012: Springer Berlin Heidelberg.
6. BOSCH. *Bosch Ignition Coils*. 2016; Available from: http://www.boschcarservice.pt/boaa-pt/Product.jsp?prod_id=70&ccat_id=32&language=en-GB&publication=1.
7. Heywood, J.B., *Internal Combustion Engine Fundamentals*. 1988: McGraw-Hill.
8. Hillier, V.A.W., *Hillier's Fundamentals of Automotive Electronics*. 1996: Stanley Thornes.
9. Tooley, M., *Electronic Circuits: Fundamentals and Applications*. 2012: Taylor & Francis.
10. Dale, J.D., M.D. Checkel, and P.R. Smy, *Application of high energy ignition systems to engines*. Progress in Energy and Combustion Science, 1997. **23**(5–6): p. 379-398.
11. Weinrotter, M., et al., *Laser ignition of ultra-lean methane/hydrogen/air mixtures at high temperature and pressure*. Experimental Thermal and Fluid Science, 2005. **29**(5): p. 569-577.
12. Lackner, M., et al., *Laser ignition in internal combustion engines-A contribution to a sustainable environment*. 2004: na.
13. Rapp, V.H., et al., *Extending Lean Operating Limit and Reducing Emissions of Methane Spark-Ignited Engines Using a Microwave-Assisted Spark Plug*. Journal of Combustion, 2012. **2012**: p. 8.
14. Srivastava, D.K. and A.K. Agarwal, *Comparative experimental evaluation of performance, combustion and emissions of laser ignition with conventional spark plug in a compressed natural gas fuelled single cylinder engine*. Fuel, 2014. **123**: p. 113-122.
15. Lancaster, D.R., et al., *Effects of turbulence on spark-ignition engine combustion*. 1976, SAE Technical Paper.
16. Davis, G.W., J. Bouboulis, and E. Heil, *The Effect of a Multiple Spark Discharge Ignition System and Spark Plug Electrode Configuration on Cold Starting of a Dedicated E85 Fueled Vehicle*. 1999, SAE Technical Paper.
17. Kito, S., et al., *Ignition limit of lean mixture by hydrogen flame jet ignition*. JSAE review, 2000. **21**(3): p. 373-378.
18. Jiang, S., *Numerical analysis of two-stroke engine with direct injection and jet ignition*. 2015.
19. Maker, P.D. and R.W. Terhune, *Study of Optical Effects Due to an Induced Polarization Third Order in the Electric Field Strength*. Physical Review, 1965. **137**(3A): p. A801-A818.
20. Ronney, P.D., *Laser versus conventional ignition of flames*. Optical Engineering, 1994. **33**(2): p. 510-521.
21. Dodd, R., et al., *Laser ignition of an IC test engine using an Nd: YAG laser and the effect of key laser parameters on engine combustion performance*. Lasers Engineering, 2007. **17**: p. 213-231.
22. Weinrotter, M., et al. *Laser ignition of engines: a realistic option!* in *International Conference on Lasers, Applications, and Technologies 2005: High-Power Lasers and Applications*. 2006. International Society for Optics and Photonics.

23. Phuoc, T.X., *Laser-induced spark ignition fundamental and applications*. Optics and Lasers in Engineering, 2006. **44**(5): p. 351-397.
24. Yalin, A.P., *High power fiber delivery for laser ignition applications*. Optics express, 2013. **21**(106): p. A1102-A1112.
25. Meek, J.M. and J.D. Craggs, *Electrical breakdown of gases*. 1978.
26. Xiao, D., *Dielectric Strength of Atmosphere Air*, in *Gas Discharge and Gas Insulation*. 2016, Springer. p. 149-194.
27. Chang, J.-S., P.A. Lawless, and T. Yamamoto, *Corona discharge processes*. IEEE Transactions on plasma science, 1991. **19**(6): p. 1152-1166.
28. Van Veldhuizen, E. and W. Rutgers, *Pulsed positive corona streamer propagation and branching*. Journal of Physics D: Applied Physics, 2002. **35**(17): p. 2169.
29. Van Veldhuizen, E. and W. Rutgers, *Corona discharges: fundamentals and diagnostics*. Invited paper, Proc. Frontiers in Low Temp. Plasma Diagn. IV, Rolduc, Netherlands, 2001: p. 40-49.
30. Schenk, A., G. Rixecker, and S. Bohne. *Results from Gasoline and CNG Engine Tests with the Corona Ignition System EcoFlash*. in *Laser Ignition Conference*. 2015. Optical Society of America.
31. Starikovskaia, S., *Plasma assisted ignition and combustion*. Journal of Physics D: Applied Physics, 2006. **39**(16): p. R265.
32. Robinson, M., *Movement of air in the electric wind of the corona discharge*. Transactions of the American Institute of Electrical Engineers, Part I: Communication and Electronics, 1961. **80**(2): p. 143-150.
33. Ieta, A., et al. *Characterization of corona wind in a modular electrode configuration*. in *Proc. ESA Annual Meeting on Electrostatics*. 2013.
34. Bellenoue, M., et al., *SPARK PLUG AND CORONA ABILITIES TO IGNITE STOICHIOMETRIC AND LEAN METHANE/AIR MIXTURES*. Combustion Science and Technology, 2007. **179**(3): p. 477-496.
35. VanVoorhies, K.L., T.J. Bonazza, and J.E. Smith, *Analysis of RF corona discharge plasma ignition*. 1992, SAE Technical Paper.
36. Bonazza, T.J., K.L. VanVoorhies, and J.E. Smith, *RF plasma ignition system concept for lean burn internal combustion engines*. 1992, SAE Technical Paper.
37. Stiles, R., G.J. Thompson, and J.E. Smith, *Investigation of a radio frequency plasma ignitor for possible internal combustion engine use*. 1997, SAE Technical Paper.
38. Pineda, D.I., J.-Y. Chen, and R.W. Dibble, *Corona discharge ignition in a single cylinder research engine under boosted conditions*. 2016.
39. Motortech. *MIC5- Ignition Controller- Operating Manual*. 2014; Available from: <http://www.gen-c.co.uk/userfiles/pdf/MOTORTECH-Manual-MIC5-01.10.023-EN-2014-04-WEB.pdf>.
40. Gas, L. "*Lower and Upper Explosive Limits for Flammable Gases and Vapors (LEL/UEL)*," 2013; 22]. Available from: <http://www.chrysalisscientific.com/pg443-Lower-LEL-Upper-UEL-Explosive-Limits.pdf>.
41. Coward, H.F. and G.W. Jones, *Limits of flammability of gases and vapors*. 1952, DTIC Document.
42. Toeg, P. *How Products Are Made*. 1994; Available from: <http://www.encyclopedia.com>.
43. Zumdahl, S.S. and D.J. DeCoste, *Chemical Principles*. 2012: Cengage Learning.
44. Maxwell, J.C., *A dynamical theory of the electromagnetic field*. Philosophical transactions of the Royal Society of London, 1865. **155**: p. 459-512.
45. McLyman, C.W.T., *Transformer and inductor design handbook*. 2016: CRC press.
46. Sadiku, M.N.O., *Elements of Electromagnetics*. 2001: Oxford University Press.
47. Hoad, R., et al., *Trends in EM susceptibility of IT equipment*. IEEE Transactions on Electromagnetic Compatibility, 2004. **46**(3): p. 390-395.
48. Jackson, J.D., *Classical electrodynamics*. 1999: Wiley.

49. Ferraris, L. and W. Chang-Yu. *EMI shielding-common problems and containment strategies*. in *Electromagnetic Compatibility Proceedings, 1997 International Symposium on*. 1997.
50. Bhatia, M.S. *A technique for depositing metal layers over large areas for EMI shielding*. in *Electromagnetic Interference and Compatibility, 1995., International Conference on*. 1995.
51. Nakamura, N., T. Baika, and Y. Shibata, *Multipoint spark ignition for lean combustion*. 1985, SAE Technical Paper.
52. Hnatiuc, B., et al., *Experimental analysis of a double-spark ignition system*. *Czechoslovak Journal of Physics*, 2006. **56**(8): p. 851-867.
53. Bernstein, T., *Electrical shock hazards and safety standards*. *IEEE Transactions on Education*, 1991. **34**(3): p. 216-222.
54. Burgett, R.R., R.E. Massoll, and D.R.V. Uum, *Relationship Between Spark Plugs and Engine-Radiated Electromagnetic Interference*. *IEEE Transactions on Electromagnetic Compatibility*, 1974. **EMC-16**(3): p. 160-172.
55. Uehara, K. and H. Takeshita, *Cutting ceramics with a technique of hot machining*. *CIRP Annals-Manufacturing Technology*, 1986. **35**(1): p. 55-58.
56. Loctite, H. *Loctite 5339- Teknisk datablad*. 2004; Available from: http://www.loctiteproducts.com/tds/EPXY_5MIN_tds.pdf.

Appendix

A.1: User Guide DRAFT

TK500 TESLACOILDRIVER

Features

- Input voltage 230VAC
- 160VDC output
- Optical input (Toslink connector)
- Power Limiter

Description

The tesla coil driver is a box with optical input, and output for driving an dual resonant tesla coil rig. The driver has an internal series load capacitor.

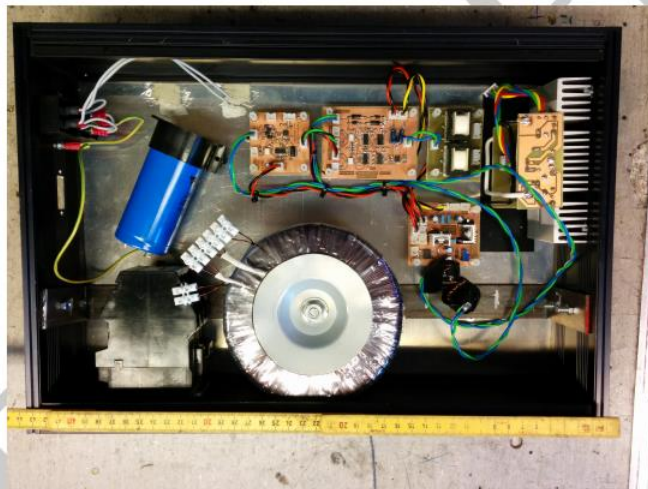


Figure 1: Product image

Contents

1	Connections	3
1.1	Optical interface	3
1.2	Tesla out	3
2	Powersupplies	5
2.1	5V	5
3	Schematics	6

Draft

1 Connections

Table 1 contains an overview of the available connections on the controller card.

Designator	Connector name	Description
J500XX	AC in	Connector for 230V in.
J500XX	Tesla out 2	Connector for connecting coil rig.
J500XX	Optical	Connector for input control signal.

Table 1: Connections on controller card

1.1 Optical interface

The tesla coil driver has a optical connector (TOSLINK) for the input control signal. The input control signal should be pulse width modulated (PWM) with a 2MHz carrier wave. The signal should have an maximal pulse width (high) of $680\mu S$. The tesla coil fires as long as the control signal is active. To adjust the length of the spark the pulse width can be adjusted. Shorter pulse width equals shorter spark. See fig. 2 for a graphical representation. In the figure 'CW' is the clock signal, 'Control Signal' is the control signal, and 'PWM' is the signal on the optical cable. Note that the aspects and pulse widths are not exact. A pulse width of 80% for active and 10% for inactive should be sufficient.

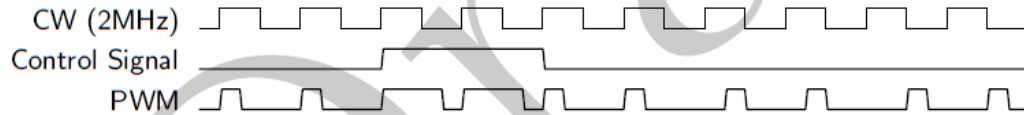


Figure 2: Control signal timing diagram

1.2 Tesla out

The tesla out connector connects to the coil rig. The coil rig schematic is shown in fig. 3. C1 is physically small and contained inside the driver enclosure. L1 is physically large and encloses L2 with a large air gap in between. L2 is physically large and contains significantly more windings than L1 (typ. 1000 times more). C2 is a capacitor consisting of the top load, and the environment around the top load. One plate can i.e. be a steel sphere, and the other plate can be the walls, roof, and floor of the room. Or something closer like a chain mail glove. The relationships between C1, L1, L2, C2 is given by eq. (1) and eq. (1). f_0 should be around $120kHz$.

$$f_0 = \frac{1}{\sqrt{L_1 \cdot C_1}} \quad (1)$$

$$f_0 = \frac{1}{\sqrt{L_2 \cdot C_2}} \quad (2)$$

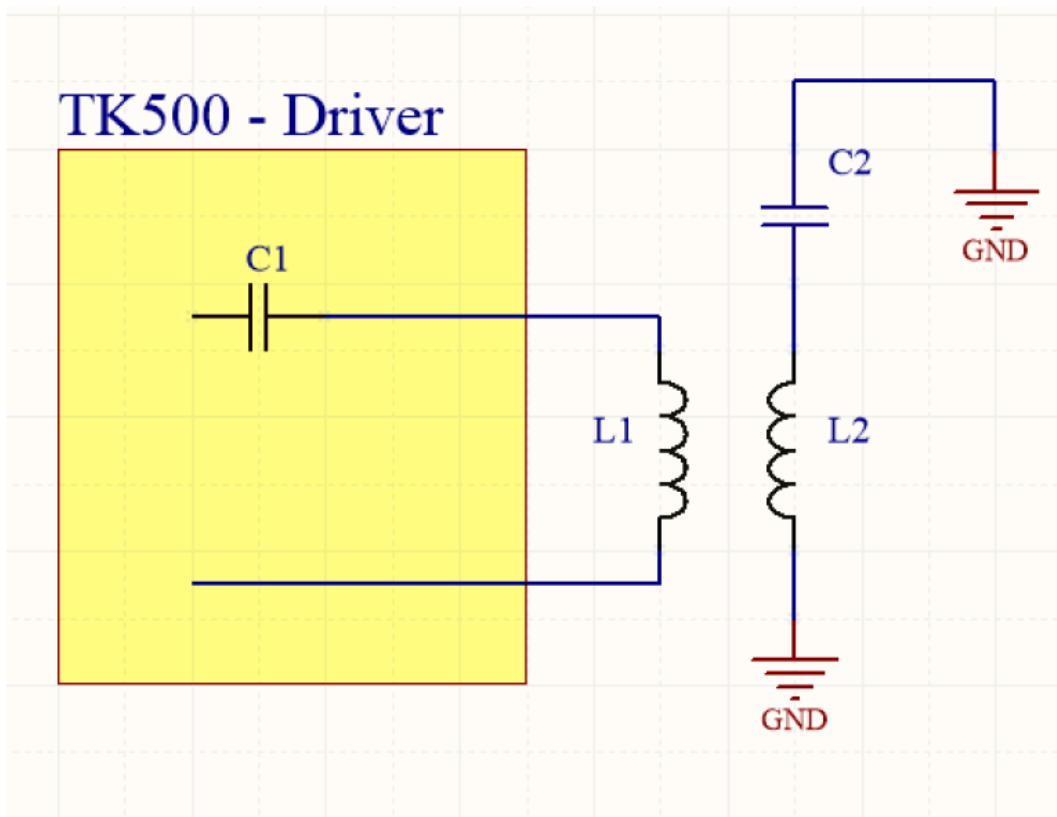


Figure 3: Coil rig schematic

A.2: Final Order Confirmation From Motortech



MOTORTECH GmbH | P.O. Box 2229 | 29262 Celle | Germany

NTNU - Norwegian University
of Science and Technology
Department of Marine Technology
Otto Nielsens vei 10
7491 Trondheim
NORWEGEN

Fax: 004773595778

Ship to:

NTNU - Norwegian University, of Science and Technology, Department of Marine Technology Otto Nielsens, 7491 Trondheim NORWEGEN

PU: O = 1 pc | 10 = 10 pcs | 100 = 100 pcs | 1K = 1000 pcs

Order Confirmation

No.: 25032034 **Original**
Date : 19.05.2015
Customer Number : 369430
Your Order No. : E-Mail Peter Sommerseth Jaer
Your order of : 27.03.2015
Our Quotation : 17009369
Person in Charge : Julian Schürmann
E-Mail : jschuermann@motortech.de
Phone : 05141 9399 -421

Page: 1

Item No.	Part Number	Del. Week	Qty Unit	Unit Price	PU	Discount	Total EUR
MIC5 Shielded Application Budget Price							
1,0	66.00.540-20 MIC5 ignition controller Heavy Duty, 20 outputs C.Tariff No.: 8511 80 00 Origin: DE Weight: 9,4700 kg	23/2015	1 ea	2.200,00	O	-25,00%	1.650,00
2,0	95.40.235-5 harness 35-pole, 180°, pin, 5 ft. C.Tariff No.: 8544 49 95 Origin: PL Weight: 0,0000 kg	23/2015	1 ea	285,00	O	-25,00%	213,75
3,0	15.07.134 Flex conduit 3/4 inch, CSA, black C.Tariff No.: 3917 32 00 Origin: DE Weight: 7,0000 kg	23/2015	2,000 m	22,00	O	-25,00%	33,00
4,0	15.07.231 fitting, 3/4 Inch C.Tariff No.: 7318 29 00 Origin: US Weight: 0,1000 kg	23/2015	1 ea	9,00	O	-25,00%	6,75
4,5	06.05.075 Junction box C.Tariff No.: 8511 90 00 Origin: DE Weight: 2,8000 kg	23/2015	1 ea	180,00	O	-25,00%	135,00
5,0	95.40.314-5 harness, 14-pole, 90°, socket, 5 ft. C.Tariff No.: 8544 49 95 Origin: PL Weight: 1,0000 kg	23/2015	1 ea	160,00	O	-25,00%	120,00
6,0	15.07.112 Flex conduit 1/2 inch, CSA, black C.Tariff No.: 3917 32 00 Origin: DE Weight: 5,2200 kg	23/2015	2,000 m	18,00	O	-25,00%	27,00
7,0	15.07.221 Fitting 1/2 Inch C.Tariff No.: 7318 29 00 Origin: US Weight: 0,0725 kg	23/2015	1 ea	5,00	O	-25,00%	3,75
8,0	000000 P/N: 95.86.205-NAN Weight: 0,0000 kg Wiring Rail shielded 2 cylinder 5 inch cylinder to cylinder distance.	23/2015	1 ea	370,00	O	-25,00%	277,50

MOTORTECH GmbH
Hogrevestr. 21 - 23
29223 Celle
Germany
www.motortech.de
motortech@motortech.de

Phone: +49 5141 9399-0
Fax: +49 5141 9399-99
Amtsgericht Lüneburg
HRB 100 364
USt-Id-Nr. DE 115117459
St-Nr. 17/202/69510

Commerzbank Celle
BLZ 257 800 22
Konto: 400 059 600 (EUR / USD)
BIC: DRESDEFF257
DE28257800220400059600

Sparkasse Celle
BLZ 257 500 01
Konto: 30 30 32 (EUR)
BIC: NOLADE21CEL
DE71257500010000303032

Hypo Vereinsbank
BLZ 200 300 00
Konto: 622 905 792 (EUR)
BIC: HYVEDEMM300
DE65200300000622905792

Geschäftsführer /
Managing Director
Florian Virchow
Robert Virchow
Mona Virchow



Order Confirmation

No.: 25032034

Date : 19.05.2015

PU: O = 1 pc | 10 = 10 pcs | 100 = 100 pcs | 1K = 1000 pcs

Page: 2

Item No.	Part Number	Del. Week	Qty	Unit	Unit Price	PU	Discount	Total EUR
9,0	95.99.200-2 AlphaRail primary lead kit for 3 pole ignition coils, shielded, externally mounted C.Tariff No.: 8536 90 10 Origin: DE Weight: 0,2500 kg	23/2015	2	ea	95,00	O	-25,00%	142,50
10,0	95.09.005 ignition coil, shielded C.Tariff No.: 8511 30 00 Origin: PL Weight: 1,5000 kg	23/2015	2	ea	170,00	O	-25,00%	255,00
11,0	000000 Shielded High Tension Lead M18 spark plug connection Weight: 0,0000 kg	23/2015	2	ea	135,00	O	-25,00%	202,50
12,0	G13-5 Spark plug M18x1.5, reach 0.750 in., hex 7/8 in., Denso Double Iridium C.Tariff No.: 8511 10 00 Origin: JP Weight: 0,1200 kg	23/2015	4	ea	74,00	O	-10,00%	266,40
13,0	000000 Shielded High Tension Lead M14 Spark plug connection Weight: 0,0000 kg	23/2015	2	ea	135,00	O	-25,00%	202,50
14,0	GE3-5 Spark plug M14x1.25, reach 0.750 in., hex 13/16 in., Denso Double Iridium C.Tariff No.: 8511 10 00 Origin: JP Weight: 0,0650 kg	23/2015	4	ea	30,00	O	-10,00%	108,00

Terms of payment: Bank transfer in advance - paid on 19/5/2015

Net values without Surcharges	3.643,65
Freight+Packing	175,00
Total Amount	EUR 3.818,65

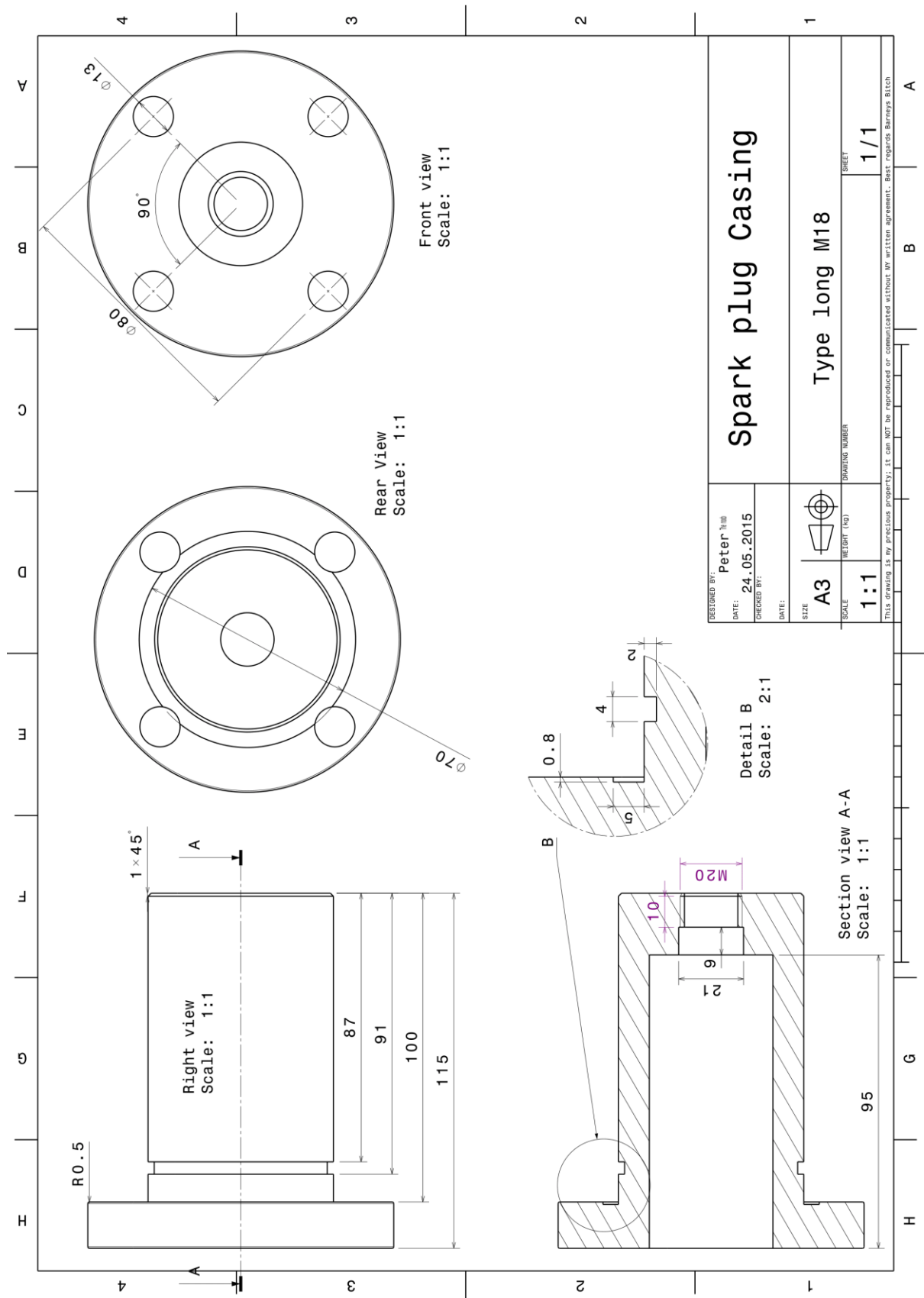
Ship via : truck
 Terms of Delivery : DAP
 Terms of Payment : Payment in advance.

All sales are based on our "General Terms of Sale" and "Software License Terms" (download at www.motortech.de) and accepted when placing the order.

Please see the appropriate product documentation for further important information.

MOTORTECH GmbH Hogrevestr. 21 - 23 29223 Celle Germany www.motortech.de motortech@motortech.de	Phone: +49 5141 9399-0 Fax: +49 5141 9399-99 Amtsgericht Lüneburg HRB 100 364 USt-Id-Nr. DE 115117459 St-Nr. 17/202/69510	Commerzbank Celle BLZ 257 800 22 Konto: 400 059 600 (EUR / USD) BIC: DRESDEFF257 DE28257800220400059600	Sparkasse Celle BLZ 257 500 01 Konto: 30 30 32 (EUR) BIC: NOLADE21CEL DE71257500010000303032	Hypo Vereinsbank BLZ 200 300 00 Konto: 622 905 792 (EUR) BIC: HYVEDEMM300 DE6520030000622905792	Geschäftsführer / Managing Director Florian Virchow Robert Virchow Mona Virchow
---	--	---	--	---	---

A.3: Technical Drawing For the M18 Rig Plug



A.4 :Gas Mixing Start Program

```
disp('Gasmixing program 3.0')
fprintf('\n')
disp('Copyright 2016, Peter Sommerseth Jaer, Marintek/NTNU')
fprintf('\n')
disp('New ambient condition inside the rig before filling')
fprintf('\n')
fprintf('\n')

% Stoichiometric reaction of CO with oxygen as oxidizer
% CO + O2 + N2 -> CO2 + N2
% The chemical reactions with excess air after combustion
% X1O2 + X2 + X3CO -> Z1O2 + Z2N2 + Z3CO2
% O: 2*X1 + 0*X2 + X3 -> 2*Z1 + 0*Z2 + Z3
% N: X2 -> Z2
% C: X3 -> Z3
% Stating all the given values

V_gas = 50;      % [dm3] Volume of the gas bottle
V_rig = 5;      % [dm3] Volume of the rig
P_gas = 40;     % [bar] Max pressure due to safety reasons.
T_gas = 293.15; % [K] Bottle temp
T_rig = 293.15; % [K] Rig temp
R_m = 8.31;     % [J/molK] General gas constant
M_o2 = 32.00;  % [g/mol] Molar mass O2
M_n2 = 28.02;  % [g/mol] Molar mass N216/28
M_co = 28.01;  % [g/mol] Molar mass CO
M_co2 = 44.01; % [g/mol] Molar mass CO2
R_o2 = 259.80; % [J/kgK] Gas constant for O2
R_n2 = 296.80; % [J/kgK] Gas constant for N2
R_co = 296.80; % [J/kgK] Gas constant for CO
R_co2 = 188.90; % [J/kgK] Gas constant for CO2
Cp_n2 = 1039;  % [j/kgK] Specific heat for N2
Cp_o2 = 913;   % [j/kgK] Specific heat for O2
Cp_co = 1039;  % [j/kgK] Specific heat for CO
Cp_co2 = 791;  % [j/kgK] Specific heat for CO2
Cp_air = 1005; % [j/kgK] Specific heat for Air
lhv_co = 282.9; % [kJ/mol] lower heating value for CO
AFRs = (M_o2/2+3.776/2*M_n2)/M_co; % [-] Stoichiometric Oxygen/fuel ratio for
complete combustion with 1/2 mole of O2
co_lfl = 12.5; % [%] lower flammability limit for CO in volume fraction

%Rig condition at atmospheric condition before filling
r_o2_ac = 21; % [%] vol% of oxygen
r_n2_ac = 79; % [%] vol% of Nitrogen
P_rig = 1; % [bar] Rig pressure
P_o2_ac = r_o2_ac/100*P_rig; % [bar] Partial pressure of O2
P_n2_ac = r_n2_ac/100*P_rig; % [bar] Partial pressure of N2
n_tot_ac = (P_rig*10^5*V_rig*10^-3)/(R_m*T_rig); % [mol] total amount of
substance
n_o2_ac = r_o2_ac/100*n_tot_ac; % [mol] amount of O2
n_n2_ac = r_n2_ac/100*n_tot_ac; % [mol] amount of N2
m_o2_ac = n_o2_ac*M_o2; % [g] mass of O2
m_n2_ac = n_n2_ac*M_n2; % [g] mass of N2
m_tot_ac = m_o2_ac+m_n2_ac; % [g] Tot amount of substance in the rig
R_rig_ac = R_o2*(m_o2_ac/m_tot_ac)+R_n2*(m_n2_ac/m_tot_ac); % [j/kgK] gas
constant of air in the rig before filling

%Setting n after the combustion in the Rig
```

```

n_co2_a = 1; % [mol] amount of substance CO2 (Z3)
m_co2_a = n_co2_a*M_co2; % [g] mass of CO2
n_n2_a = 2.31; % [mol] amount of substance N2 (Z2)
m_n2_a = n_n2_a*M_n2; % [g] mass of N2
r_o2_a = 21; % [%] vol% of O2 after combustion
n_o2_a = r_o2_a/100 *(n_co2_a+n_n2_a)/(1-r_o2_a/100); % [mol] amount of
substance O2 (Z1)
r_co2_a = n_co2_a/(n_n2_a+n_o2_a+n_co2_a)*100; % [%] Vol% of CO2 after
combustion
r_n2_a = n_n2_a/(n_n2_a+n_o2_a+n_co2_a)*100; % [%] Vol% of N2 after
combustion
m_o2_a = n_o2_a*M_o2; % [g] mass of O2 after combustion
m_tot_a = m_o2_a+m_co2_a+m_n2_a; % [g] total amount of substance after pre
combustion
R_ges_a = % [J/kgK] Gas constant for mixture after pre combustion
R_o2*(m_o2_a/m_tot_a)+R_co2*(m_co2_a/m_tot_a)+R_n2*(m_n2_a/m_tot_a);
Cp_a = % [j/kgK] Specific heat for the mixture
Cp_o2*(m_o2_a/m_tot_a)+Cp_n2*(m_n2_a/m_tot_a)+Cp_co2*(m_co2_a/m_tot_a);
m_tot_a = m_co2_a + m_n2_a +m_o2_a; % [g] total amount of substances after
combustion
mf_co2_a = (m_co2_a / m_tot_a)*100 ; % [%] mass fraction of CO2
mf_n2_a = (m_n2_a / m_tot_a)*100 ; % [%] mass fraction of N2
mf_o2_a = (m_o2_a / m_tot_a)*100 ; % [%] mass fraction of O2

%Before Combustion in the Rig
n_co = n_co2_a; % [mol] amount of CO X3 before combustion
m_co = M_co*n_co; % [g] Mass of substance CO X3 before combustion
n_n2 = n_n2_a; % [mol] amount of N2 X2 before combustion
m_n2 = n_n2*M_n2; % [g] Mass of substance N2 X2 before combustion
n_o2 = n_o2_a+n_co2_a-n_co/2; % [mol] amount of O2 X1 before combustion
m_o2 = n_o2*M_o2; % [g] Mass of substance O2 X1 before combustion
m_tot = m_o2+m_n2+m_co; % [g] Total mass of substance before combustion
r_o2 = n_o2/(n_o2+n_n2+n_co)*100; % [%] Vol% of O2 before combustion
r_co = n_co/(n_o2+n_n2+n_co)*100; % [%] Vol% of CO before combustion
r_n2 = n_n2/(n_o2+n_n2+n_co)*100; % [%] Vol% of N2 before combustion
R_ges = R_o2*(m_o2/m_tot)+R_n2*(m_n2/m_tot)+R_co*(m_co/m_tot); % [J/kgK] Gas
constant for mixture before pre combustion
Cp = Cp_o2*(m_o2/m_tot)+Cp_n2*(m_n2/m_tot)+Cp_co*(m_co/m_tot); % [j/kgK]
Specific heat for the mixture
mf_o2 = (m_o2/m_tot)*100; % [%] Mass fraction of O2 before combustion
mf_co = (m_co/m_tot)*100; % [%] Mass fraction of CO before combustion
mf_n2 = (m_n2/m_tot)*100; % [%] Mass fraction of N2 before combustion

%Gas Bottle Before filling contains the mixture from prevoius filling
P_bottle_bf = 1; % [bar] bottle pressure
P_o2_bottle_bf = P_bottle_bf*(r_o2/100); % [bar] partial pressure of O2
P_n2_bottle_bf = P_bottle_bf*(r_n2/100); % [bar] partial pressure of N2
P_co_bottle_bf = P_bottle_bf*(r_co/100); % [bar] partial pressure of CO
r_o2_bottle_bf = P_o2_bottle_bf/P_bottle_bf*100; % [%] Volume fraction of O2
r_n2_bottle_bf = P_n2_bottle_bf/P_bottle_bf*100; % [%] Volume fraction of N2
r_co_bottle_bf = P_co_bottle_bf/P_bottle_bf*100; % [%] Volume fraction of CO
n_tot_bottle_bf = ((P_bottle_bf*10^5*50*10^-3)/(R_m*T_gas)); % [mol] Amount
of substance in the bottle
n_o2_bottle_bf = n_tot_bottle_bf*r_o2_bottle_bf/100; % [mol] Amount of O2 in
the bottle
n_n2_bottle_bf = n_tot_bottle_bf*r_n2_bottle_bf/100; % [mol] Amount of N2 in
the bottle

```

```

n_co_bottle_bf = n_tot_bottle_bf*r_co_bottle_bf/100; % [mol] Amount of CO in
the bottle
m_o2_bottle_bf = M_o2*n_o2_bottle_bf; % [g] Mass of O2
m_n2_bottle_bf = M_o2*n_n2_bottle_bf; % [g] Mass of N2
m_co_bottle_bf = M_o2*n_co_bottle_bf; % [g] Mass of CO
m_tot_bottle_bf = m_o2_bottle_bf+m_n2_bottle_bf+m_co_bottle_bf; % [g] Total
Mass

% Added components to Gas Bottle after filling to gas mixing bottle
T_bottle_af = T_gas; % [K] temperature of the bottle after filling
n_bottle_ad = (P_gas-P_bottle_bf)*10^5*V_gas*10^-3/(R_m*T_bottle_af); %
[mol] Amount of substance added to the bottle from atmospheric conditions to
40 bar
n_o2_aaf = n_bottle_ad*(r_o2/100); % [mol] Amount of O2
n_n2_aaf = n_bottle_ad*(r_n2/100); % [mol] Amount of N2
n_co_aaf = n_bottle_ad*(r_co/100); % [mol] Amount of CO
m_o2_aaf = n_o2_aaf*M_o2; % [g] Mass of O2
m_n2_aaf = n_n2_aaf*M_n2; % [g] Mass of N2
m_co_aaf = n_co_aaf*M_co; % [g] Mass of CO
P_o2_aaf = n_o2_aaf*R_m*T_bottle_af/(V_gas*10^-3)*10^-5; % [bar] Partial
pressure of O2
P_n2_aaf = n_n2_aaf*R_m*T_bottle_af/(V_gas*10^-3)*10^-5; % [bar] Partial
pressure of N2
P_co_aaf = n_co_aaf*R_m*T_bottle_af/(V_gas*10^-3)*10^-5; % [bar] Partial
pressure of CO
r_o2_aaf =n_o2_aaf/n_bottle_ad*100; % [%] Vol% of O2
r_n2_aaf =n_n2_aaf/n_bottle_ad*100; % [%] Vol% of N2
r_co_aaf =n_co_aaf/n_bottle_ad*100; % [%] Vol% of CO

%Gasmixing filling procedure with old mix inside CO-->N2-->O2= 40 bar due to
safety reasons
%and end state of components inside gas bottle
P_co_bottle_f = P_o2_bottle_bf+P_n2_bottle_bf+P_co_bottle_bf+P_co_aaf; %
[bar] Filling pressure of CO
P_n2_bottle_f = P_co_bottle_f+P_n2_aaf; % [bar]Filling pressure of N2
P_o2_bottle_f = P_n2_bottle_f+P_o2_aaf;% [bar]Filling pressure of O2
n_o2_bottle_af = n_bottle_ad*(r_o2/100)+n_o2_bottle_bf; % [mol] Total amount
of O2
n_n2_bottle_af = n_bottle_ad*(r_n2/100)+n_n2_bottle_bf; % [mol] Total amount
of N2
n_co_bottle_af = n_bottle_ad*(r_co/100)+n_co_bottle_bf; % [mol] Total amount
of CO
m_o2_bottle_af = n_o2_bottle_af*M_o2; % [g] Mass of O2
m_n2_bottle_af = n_n2_bottle_af*M_n2; % [g] Mass of N2
m_co_bottle_af = n_co_bottle_af*M_co; % [g] Mass of CO
P_o2_bottle_af = n_o2_bottle_af*R_m*T_bottle_af/(V_gas*10^-3)*10^-5; % [bar]
Partial pressure of O2
P_n2_bottle_af = n_n2_bottle_af*R_m*T_bottle_af/(V_gas*10^-3)*10^-5; % [bar]
Partial pressure of N2
P_co_bottle_af = n_co_bottle_af*R_m*T_bottle_af/(V_gas*10^-3)*10^-5; % [bar]
Partial pressure of CO
P_bottle_af = P_co_bottle_af+P_n2_bottle_af+P_o2_bottle_af; % [Bar] Total
pressure of bottle after filling
r_o2_bottle_af =n_o2_bottle_af/n_bottle_ad*100; % [%] Vol% of O2
r_n2_bottle_af =n_n2_bottle_af/n_bottle_ad*100; % [%] Vol% of N2
r_co_bottle_af =n_co_bottle_af/n_bottle_ad*100; % [%] Vol% of CO

%the rig condition after filling:
prompt = ' What pressure is set in the rig ? ';
P_rig_arf = input(prompt); % [bar] rig pressure
T_rig_arf = 293.15; % [K] Rig temperature

```

```

r_o2_rig_arf = r_o2_aaf; % [%] volume fraction of O2
r_n2_rig_arf = r_n2_aaf; % [%] volume fraction of N2
r_co_rig_arf = r_co_aaf; % [%] volume fraction of CO
n_tot_rig_arf = n_o2_ac+n_n2_ac+(((P_rig_arf-P_rig)*10^5*5^-3)/(R_m*T_rig));
% [mol] Tot amount of substance after filling
n_o2_rig_arf = n_tot_rig_arf*r_o2_rig_arf/100; % [mol] Amount of O2
n_n2_rig_arf = n_tot_rig_arf*r_n2_rig_arf/100; % [mol] Amount of N2
n_co_rig_arf = n_tot_rig_arf*r_co_rig_arf/100; % [mol] Amount of CO
P_o2_rig_arf = r_o2_rig_arf*P_rig_arf/100; % [Bar] Partial pressure of
O2
P_n2_rig_arf = r_n2_rig_arf*P_rig_arf/100; % [Bar] Partial pressure of
n2
P_co_rig_arf = r_co_rig_arf*P_rig_arf/100; % [Bar] Partial pressure of
CO
m_o2_rig_arf = n_o2_rig_arf*M_o2; % [g] Mass of O2
m_n2_rig_arf = n_n2_rig_arf*M_n2; % [g] Mass of N2
m_co_rig_arf = n_co_rig_arf*M_co; % [g] Mass of O2 10
m_tot_rig_arf = m_o2_rig_arf+m_n2_rig_arf+m_co_rig_arf; % [g] Mass of all
substance
R_gas_rig_arf =
R_o2*r_o2_rig_arf/100+R_n2*r_n2_rig_arf/100+R_co*r_co_rig_arf/100; % [J/kgK]
Gas constant for mixture befor pre combustion
Cp_gas_rig_arf =
Cp_o2*(m_o2_rig_arf/m_tot_rig_arf)+Cp_n2*(m_n2_rig_arf/m_tot_rig_arf)+Cp_co
*(m_co_rig_arf/m_tot_rig_arf); % [J/kgK] Spesific heat for mixture
E_rig_arf = lhv_co*n_co_rig_arf; % [kj] Amount of energy in the rig of
CO
AFR_rig_arf = m_o2_rig_arf/m_co_rig_arf; % [-] Air/fuel ratio for rig after
filling
Lambda_rig_arf = AFR_rig_arf/AFRs ; % [-] The relative air fuel ratio

%DISPING TIME:)
disp('The mixing bottle contains a mixture of O2,N2 and CO at atmosferic
conditions before filling and should be filled up in the following order in
Bar')
disp('Carbondioxide')
disp(P_co_bottle_f)
disp('Nitrogen')
disp(P_n2_bottle_f)
disp('oxygen')
disp(P_o2_bottle_f)
disp('corresponing volume fraction for each component is as follows')
disp('CO')
disp(r_co_bottle_af)
disp('N2')
disp(r_n2_bottle_af)
disp('O2')
disp(r_o2_bottle_af)
disp('Which correspond to the following partial pressures of each component
in the tank')
disp('CO')
disp(P_co_bottle_af)
disp('N2')
disp(P_n2_bottle_af)
disp('O2')
disp(P_o2_bottle_af)
disp('which gives a total bottle pressure of')
disp(P_bottle_af)

```

A.5: Out Leaning Program

```
run gasmixstart

prompt = ' What pressure is left in the mixing tank in bar? ';
P_bottle_as = input(prompt); % [Bar] Remaining pressure in mixing bottle
after n rig fillings
disp( ' The previous volume fraction of CO was ');
disp(r_co_bottle_af);
prompt = ' What is desired volume fraction of CO in the mixture in Bar? ';
fprintf('\n')
fprintf('\n')

r_co_bottle_as1 = input(prompt); % [vol%] Desired volume
fraction of CO in the mixing bottle
P_o2_bottle_as = P_bottle_as*(r_o2_bottle_af/100); % [Bar] Partial pressure
of O2
P_n2_bottle_as = P_bottle_as*(r_n2_bottle_af/100); % [Bar] Partial pressure
of N2
P_co_bottle_as = P_bottle_as*(r_co_bottle_af/100); % [Bar] Partial pressure
of CO
P_co_bottle_as1 = P_bottle_as*(r_co_bottle_as1/100); % [Bar] Correspondig
partial pressure for desired CO volume fraction

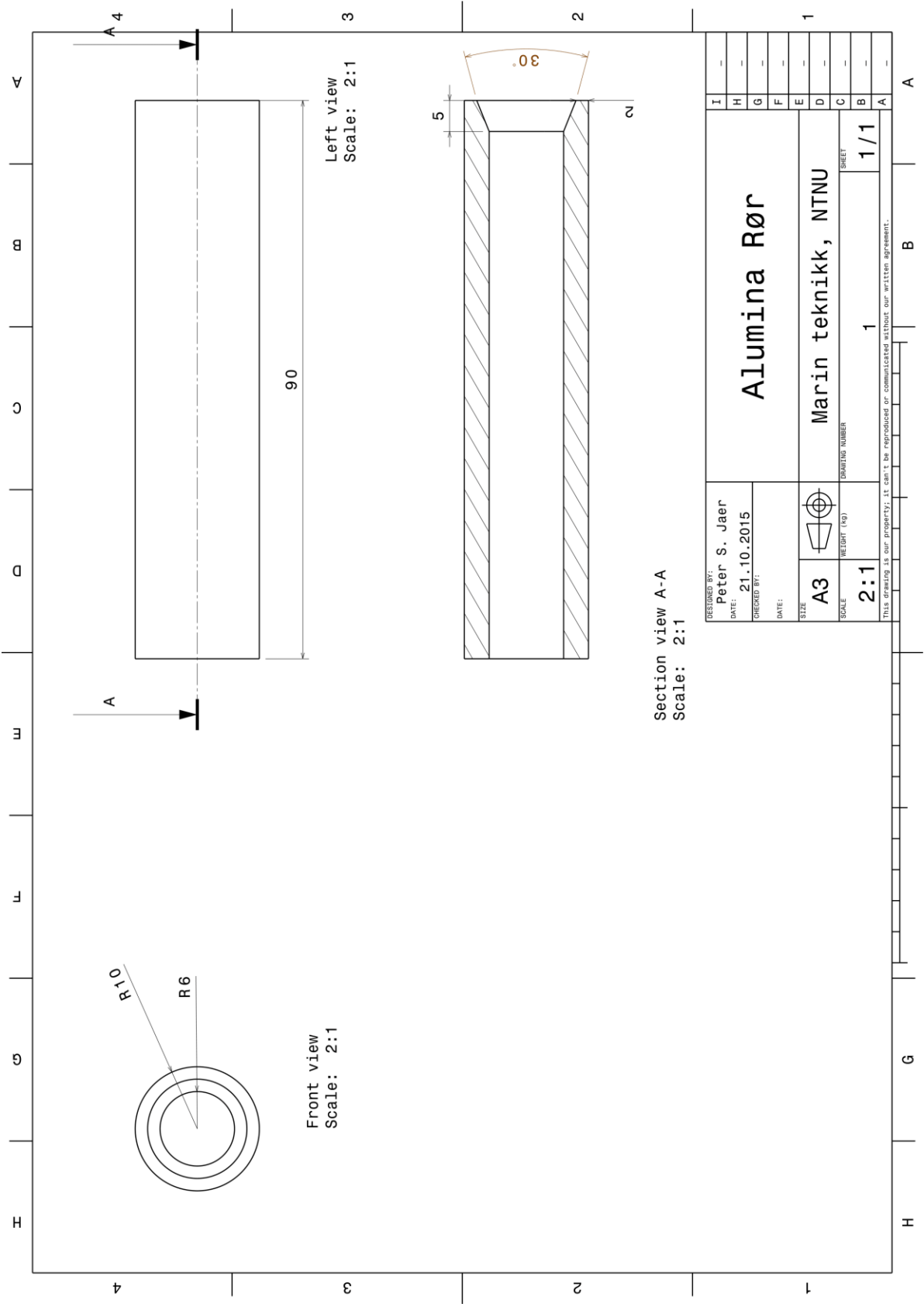
P_n2_bottle_tba = (P_co_bottle_as/r_co_bottle_as1*100)-P_bottle_as; % [bar]
Partial pressure of N2 to be added to the mixing tank
P_n2_bottle_tot = P_n2_bottle_tba + P_n2_bottle_as ; % [bar]
total partial pressure of N2 in the mixing tank
r_n2_bottle_as1 = P_n2_bottle_tot/(P_bottle_as+P_n2_bottle_tba) *100; % [vol
%] Volume fraction of N2
r_o2_bottle_as1 = P_o2_bottle_as/(P_bottle_as+P_n2_bottle_tba) *100; % [vol
%] Volume fraction of O2
r_co_bottle_as1 = P_co_bottle_as/(P_bottle_as+P_n2_bottle_tba)*100; % [vol
%] Volume fraction of CO

P_bottle_aan = P_n2_bottle_tba +P_bottle_as ; % [bar] total pressure
in tank after added Nitrogen
P_co_bottle_aan = P_bottle_aan*(r_co_bottle_as1/100) ; % [Bar] Partial
pressure of CO in mixing bottle
P_n2_bottle_aan = P_bottle_aan*(r_n2_bottle_as1/100) ; % [Bar] Partial
pressure of n2 in mixing bottle
P_o2_bottle_aan = P_bottle_aan*(r_o2_bottle_as1/100) ; % [Bar] Partial
pressure of O2 in mixing bottle
P_bottle_tot_aan=P_co_bottle_aan+P_n2_bottle_aan+P_o2_bottle_aan;

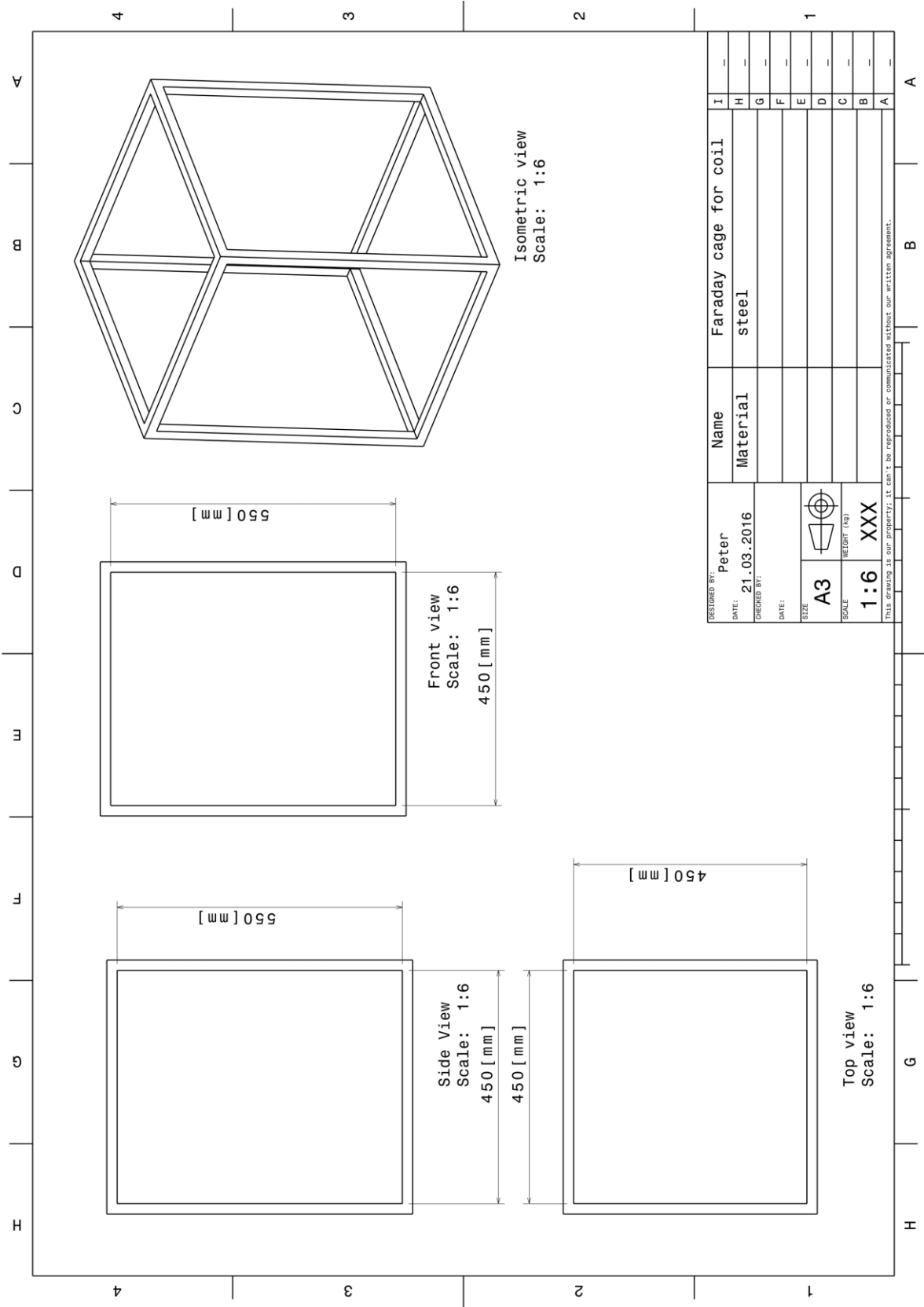
disp('Filling pressure in the mixing tank by adding N2')
disp(P_bottle_aan);
fprintf('\n')
fprintf('\n')
disp('Which means that the following amount of N2 is added ')
disp(P_n2_bottle_tba);
disp('partial pressure of CO')
disp(P_co_bottle_aan)
disp('partial pressure of N2')
disp(P_n2_bottle_aan)
disp('partial pressure of O2')
disp(P_o2_bottle_aan)
disp(P_bottle_tot_aan)
```

```
disp('And a total volume fraction of CO of')  
disp(r_co_bottle_asl)
```


A.6: Technical Drawing of Alumina Tube



A.7: Technical Drawing of Faraday Cage



A.8: MP104

Measure Protocol 104										Leaning out	
Keyword											
Protocol number 104											
Injector NO											
Nozzle NO											
Injector number -											
Spark plug position changed, No Heating elements											
Q100	-	[ml/min]	Lens opening	5,6		[-]					
Nozzle Diameter	-	[mm]	Full load quantity	-		[mm3]					
Number of holes	-	[-]	Injection Temp	-		[°C]					
Spray angle	-	[°]	Calc. Injection time	-		[s]					
Room temp.	22	[°C]	Shutter time	1/25000		1/pic					
Fuel Density	-	[kg/dm3]									
Fuel Pressure	-	bar									
Frame Rate	500	p/s	Time of P-r starts	0		s/ to ignition					
Resolution	640x544	[-]									
Point	Rig load	vol fraction of CO	Energy content	Lens opening	Shutter Timing	Heating (P/H)	fan timing		fan Speed	Spark plug	
[-]	[bar]	[%]	[kJ]	[-]	[1/pic]	[-]	[s]	[s]	[rpm]	[-]	
✓ 1	8,50	20,04	2191	5,60	1/25000	0/0	0	0	0,00	9/4	Gust P 34 36,2
✓ 2	8,50	19,63	2189	5,60	1/25000	0/0	0	0	0,00	9/4	
✓ 3	8,50	19,21	2187	5,60	1/25000	0/0	0	0	0,00	9/4	
✓ 4	8,50	18,79	2185	5,60	1/25000	0/0	-10	-10	1000,00	9/4	
✓ 5	8,50	18,37	2183	5,60	1/25000	0/0	-10	-10	1000,00	9/4	
6	8,50	17,74 17,94	2182	5,60	1/25000	0/0	-10	-10	1000,00	9/4	
7	8,50	17,52	2180	5,60	1/25000	0/0	18	18	1000,00	9/4	
8	8,50	17,10	2178	5,60	1/25000	0/0	18	18	1000,00	9/4	
9	8,50	16,68	2176	5,60	1/25000	0/0	18	18	1000,00	9/4	
10	8,50	16,25	2174	5,60	1/25000	0/0	18	18	1000,00	9/4	
11	8,50	15,83	2172	5,60	1/25000	0/0	18	18	1000,00	9/4	
12	8,50	15,40	2170	5,60	1/25000	0/0	18	18	1000,00	9/4	
13	8,50	14,97	2169	5,60	1/25000	0/0	18	18	1000,00	9/4	
14	8,50	14,55	2167	5,60	1/25000	0/0	18	18	1000,00	9/4	
15	8,50	14,12	2165	5,60	1/25000	0/0	18	18	1000,00	9/4	
16	8,50	13,69	2163	5,60	1/25000	0/0	18	18	1000,00	9/4	
17	8,50	13,26	2161	5,60	1/25000	0/0	18	18	1000,00	9/4	
18	8,50	12,83	2159	5,60	1/25000	0/0	18	18	1000,00	9/4	
19	8,50	12,40	2157	5,60	1/25000	0/0	18	18	1000,00	9/4	
20	8,50	11,97	2155	5,60	1/25000	0/0	18	18	1000,00	9/4	
21	8,50	11,54	2154	5,60	1/25000	0/0	18	18	1000,00	9/4	
22	8,50	11,10	2152	5,60	1/25000	0/0	18	18	1000,00	9/4	
23	8,50	10,67	2150	5,60	1/25000	0/0	18	18	1000,00	9/4	
24	8,50	10,24	2148	5,60	1/25000	0/0	18	18	1000,00	9/4	
25	8,50	9,80	2146	5,60	1/25000	0/0	18	18	1000,00	9/4	
Commer											
Test driv Peter Sommerseth Jaer											

- 1) Ignition at 4 only.
- 2) Same CO Vol% as I
- 3) according to the MP $\text{CO} = 19,21\%$ - sp. 9-4 P=36,3 bar
- 4) same as 3, but sp-6
- 5) CO Vol% = 17,74 P=33,9 (from 32,4)
- 6) CO vol% = 15,85 P=32,4 (from 30,8)
- 7) same as 6
- 8) same as 6
- 9) CO Vol% = 14 P=31 (from 29)

A.9: Calculations of Gas Composition After Gas Leaning

	outleaning process			
	1	2	3	4
Number of fillings of N2	40	34	32,8	30,8
Pressure history [Bar]	40	34,7	33,9	32,4
Pressure after filling	9,18	7,80	7,38	6,70
P_CO	18,69	16,59	16,78	16,84
P_N2	12,13	10,31	9,75	8,85
r_CO	22,95	22,49	21,76	20,68
r_N2	46,725	47,80	49,49	51,99
r_O2	30,325	29,71	28,75	27,33
Added N2 [bar]	0	0,7	1,1	1,6
Successful ignition	Yes	Yes	Yes	Yes
	40			
Filling procedure				
CO	10,18			
N2	28,08		3,4	
O2	40			
Bottle contains				
N2	0,79			
O2	0,21			

